Re-programming of GM-CSF-dependent alveolar macrophages through GSK3 activity modulation

Israel Ríos[1], Cristina Herrero[1], Mónica Torres-Torresano[2], Baltasar López-Navarro[2], María Teresa Schiaffino[2], Francisco Díaz-Crespo[3], Alicia Nieto-Valle[4], Rafael Samaniego[4], Yolanda Sierra-Palomares[5], Eduardo Oliver[5], Fernando Revuelta-Salgado[6], Ricardo García-Luján[6], Paloma Sánchez-Mateos[4,7], Rafael Delgado[8,9], Amaya Puig-Kröger[2#*] , Ángel L. Corbí[1#*].

[1] Myeloid Cell Laboratory, Centro de Investigaciones Biológicas, CSIC, Madrid, Spain.

[2] Unidad de Inmuno-Metabolismo e Inflamación, Instituto de Investigación Sanitaria Gregorio Marañón (IiSGM), Hospital General Universitario Gregorio Marañón, Madrid, Spain.

[3] Servicio de Anatomía Patológica, Hospital General Universitario Gregorio Marañón, Madrid, Spain.

[4] Unidad de Microscopía Confocal, Instituto de Investigación Sanitaria Gregorio Marañón (IiSGM), Hospital General Universitario Gregorio Marañón, Madrid, Spain.

[5] Experimental Pharmacology and New Tragets in Cardiopulmonary Disorders, Centro de Investigaciones Biológicas, CSIC, Madrid, Spain.

[6] Servicio de Neumología. Hospital Universitario 12 de Octubre. Madrid, Spain.

[7] Department of Immunology, Ophthalmology and ENT, Universidad Complutense School of Medicine, Madrid, Spain.

[8] Instituto de Investigación Hospital Universitario 12 de Octubre (imas12), Madrid, Spain.

[9] Universidad Complutense School of Medicine, Madrid, Spain.

# APK and ALC contributed equally to this work.

* Corresponding authors: Dr. Ángel L. Corbí (acorbi@cib.csic.es). Centro de Investigaciones Biológicas "Margarita Salas", CSIC. Ramiro de Maeztu, 9. Madrid 28040; Phone: 34-91-8373112; Dr. Amaya Puig-Kröger (amaya.puig@iisgm.com). Unidad de Inmuno-Metabolismo e Inflamación, Instituto de Investigación Sanitaria Gregorio Marañón (IiSGM), Madrid, Spain. Phone: 34-91-4269268.

SUMMARY

Monocyte-derived macrophages recruited into inflamed tissues can acquire an array of functional states depending on the extracellular environment. Since the anti-inflammatory/pro-fibrotic macrophage profile is determined by MAFB, whose activity/protein levels are regulated by GSK3, we addressed the macrophage re-programming potential of GSK3 modulation. GM-CSF-dependent (GM-MØ) and M-CSF-dependent monocyte-derived macrophages (M-MØ) exhibited distinct levels of inactive GSK3, and inhibiting GSK3 in GM-MØ led to acquisition of transcriptional, phenotypic and functional properties characteristic of M-MØ (enhanced expression of IL-10 and monocyte-recruiting factors, and higher efferocytosis). These re-programming effects were also observed upon GSK3α/β knockdown, and through GSK3 inhibition in *ex vivo* isolated human alveolar macrophages (AMØ). Notably, GSK3 downmodulation potentiated the transcriptional signature of Interstitial Macrophages (IMØ) while suppressed the AMØ-specific gene profile. Indeed, heightened levels of inactive GSK3 and MAFB-dependent proteins were observed in severe COVID-19 patients lung macrophages, highlighting the GSK3-MAFB axis as a therapeutic target for macrophage re-programming.

47 **INTRODUCTION**

48 Macrophages exhibit considerable functional plasticity during inflammatory responses,
49 transitioning from pro-inflammatory activities to tissue repair and inflammation resolution [1,2]. This
50 functional versatility of macrophages is intrincately tied to factors such as their ontogeny (fetal
51 origin vs. monocyte-derived) and the specific tissue and extracellular environment [3–5]. Notably,
52 monocyte-derived macrophages are oppositely instructed by M-CSF or GM-CSF [6–12]. GM-CSF directs
53 monocyte-derived macrophages (GM-MØ) towards heightened pro-inflammatory activity [10,13–15]
54 and the acquisition of the lung alveolar macrophage phenotype and gene profile [16]. In fact, GM-CSF
55 is essential for generating lung alveolar macrophages [17], crucial for surfactant homeostasis, whereas
56 deficient GM-CSF signaling leads to pulmonary alveolar proteinosis [18], a condition marked by
57 defective surfactant clearance and disruption of pulmonary homeostasis due to alveolar
58 macrophage dysfunction [19]. Conversely, M-CSF gives rise to anti-inflammatory, pro-resolving, and
59 immunosuppressive monocyte-derived macrophages (M-MØ) [1,2,20] but promotes the development
60 of pro-fibrotic pathogenic monocyte-derived macrophages in lung pathologies like idiopathic
61 pulmonary fibrosis (IPF) [21] and severe COVID-19 [22]. The pathological relevance of GM-MØ and M-
62 MØ subsets is evident in severe COVID-19, with a huge increase in monocyte-derived M-MØ and a
63 reduction of tissue-resident GM-MØ-like lung macrophages [23–25].

64

65 Despite their crucial role in maintaining tissue homeostasis, deregulated macrophage functional
66 specialization contributes to various human diseases, including tumors and chronic inflammatory
67 pathologies [26]. Consequently, macrophage re-programming has emerged as a promising therapeutic
68 approach [26]. However, achieving this necessitates a profound understanding of the transcriptional
69 and signaling mechanisms governing the pro- and anti-inflammatory nature of macrophages. In this
70 regard, recent findings indicate that the homeostatic and reparative transcriptional profile of human

71 M-MØ is orchestrated by MAF and MAFB [27–29], closely related transcription factors that regulate
72 stemness and self-renewal in the mouse haematopoietic lineage [3031,3233–35]. In fact, the distinctive
73 expression of MAFB in M-MØ, influencing IL-10 production [27,36], also mediates macrophage re-
74 programming induced by methotrexate [37] and LXR ligands [38].
75
76 Given the pivotal role of MAFB/MAF in human macrophage functional specification, and considering
77 the regulation of large MAF factors through GSK3-mediated phosphorylation-induced proteasomal
78 degradation [30], we hypothesized that modulating GSK3 activity could offer a viable avenue for re-
79 programming monocyte-derived macrophages. Our findings reveal significant differences in
80 inhibitory phosphorylation of GSK3β (Ser^9-GSK3β) and GSK3α (Ser^{21}-GSK3α) between M-MØ and
81 GM-MØ, and that GSK3 inhibition (using CHIR-99021) or knock-down (using siRNA) in GM-MØ
82 prompts the adoption of transcriptional, phenotypic, and functional characteristics resembling
83 those of M-MØ. This re-programming effect was manifested in elevated expression of IL-10,
84 monocyte-recruiting chemokines, pro-fibrotic factors, as well as in enhanced phagocytic capability,
85 all correlating with increased MAFB expression. The re-programming action of GSK3 inhibition was
86 also observed in control monocytes and in monocytes exposed to a pathological pro-inflammatory
87 environment. Importantly, GSK3 inhibition in *ex vivo* isolated human Alveolar Macrophages (AMØ),
88 led to the loss of the AMØ gene signature and the acquisition of the gene profile that characterizes
89 Interstitial Macrophages (IMØ). Since pathogenic lung macrophages in severe COVID-19 exhibit high
90 levels of inactive GSK3 and heightened levels of MAFB and MAFB-dependent proteins, our results
91 underscore the potent macrophage re-programming impact of GSK3 inhibition, and highlight the
92 GSK3-MAFB axis as a promising therapeutic target for macrophage re-programming.

93 **EXPERIMENTAL PROCEDURES**

94 **Generation of human monocyte-derived macrophages *in vitro* and treatments**. Human Peripheral
95 Blood Mononuclear Cells (PBMCs) were isolated from buffy coats from anonymous healthy donors
96 over a Lymphoprep (Nycomed Pharma) gradient according to standard procedures. Monocytes
97 were purified from PBMC by magnetic cell sorting using anti-CD14 microbeads (Miltenyi Biotec).
98 Monocytes (>95% $CD14^+$ cells) were cultured at 0.5 x 10^6 cells/ml in Roswell Park Memorial Institute
99 (RPMI 1640, Gibco) medium supplemented with 10% fetal bovine serum (FBS, Biowest) (complete
100 medium) for 7 days in the presence of 1000 U/ml GM-CSF or 10 ng/ml M-CSF (ImmunoTools) to
101 generate GM-CSF-polarized macrophages (GM-MØ) or M-CSF-polarized macrophages (M-MØ),
102 respectively [27]. Cytokines were added every two days and cells were maintained at 37°C in a
103 humidified atmosphere with 5% CO_2 and 21% O_2. Alveolar macrophages (AMØ) were obtained from
104 remains of bronchoalveolar lavage (BAL) of patients undergoing bronchoscopy for diagnostic
105 purposes under a protocol approved by the Internal Review Board of Instituto de Investigación
106 Hospital 12 de Octubre (Reference TP24/0183). BAL procedure was performed with a flexible
107 bronchoscope and a total volume of 150 ml of sterile isotonic saline solution at 37°C. BAL fluid
108 fractions were maintained at 4°C and cellular debris removed using a 40 µm cell strainer. BAL cells
109 were washed with PBS, centrifuged and resuspended in complete medium containing 100 U/mL
110 penicillin and 100 µg/mL streptomycin (#15140-122,Gibco), 50 µg/ml gentamicin (#G1397, Sigma-
111 Aldrich), and 2.5 µg/ml amphotericin B (#A2942, Sigma-Aldrich). The cells were seeded at 6–8 × 10^5
112 cells per well in 12-well plates for 1 h and washed extensively to remove non-adherent cells. Finally,
113 2 ml of complete medium with antibiotics was added to each well and the adherent cells incubated
114 for 16–18 h before treatments. More than 95% of adherent BAL cells were identified as AMØ
115 according to morphology and phenotypic analysis. When indicated, monocytes, GM-MØ or AMØ
116 were exposed to the GSK3 inhibitors CHIR99021 (10 µM), SB-216763 (10 µM) or LiCl (10 mM), using

117 DMSO as control. For macrophage activation, cells were treated with either 100 ng/ml CL264
118 (InvivoGen), 10 ng/ml *E. coli* 0111:B4 lipopolysaccharide (LPS-EB Ultrapure, Invivogen), TNF (20
119 ng/ml, ImmunoTools) or IFNγ (5 ng/ml, ImmunoTools). Human cytokine production was measured
120 in M-MØ culture supernatants using commercial ELISA [CCL2 (BD Biosciences), IL-10, CCL18, LGMN,
121 SPP1 (R&D Systems) and activin A (BD Biosciences)] and following the procedures supplied by the
122 manufacturers.

123 **siRNA transfection**. GM-MØ (1×10^6 cells) were transfected with a human *GSK3A*-specific and/or
124 *GSK3B*-specific siRNA (50 nM) (Dharmacon) using HiPerFect (Qiagen). Silencer Select Negative
125 Control No. 2 siRNA (siCtrl, 50 nM) (Dharmacon) was used as negative control siRNA. Six hours after
126 transfection, cells were either allowed to recover from transfection in complete medium (66 hours),
127 and lysed. Knockdown of GSK3α/β was confirmed by Western blot.

128 **Quantitative real-time RT-PCR (qRT-PCR)**. Total RNA was extracted using the total RNA and protein
129 isolation kit (Macherey-Nagel). RNA samples were reverse-transcribed with High-Capacity cDNA
130 Reverse Transcription reagents kit (Applied Biosystems) according to the manufacturer's protocol.
131 Real-time quantitative PCR was performed with LightCycler® 480 Probes Master (Roche Life
132 Sciences) and Taqman probes on a standard plate in a Light Cycler® 480 instrument (Roche
133 Diagnostics). Gene-specific oligonucleotides (*IL10*: Forward, 5´-TCACTCATGGCTTTGTAGATGC-3´,
134 and Reverse, 5´- GTGGAGCAGGTGAAGAATGC-3´; *LGMN*: Forward, 5´-GAACACCAATGATCTGGAGGA-
135 3´, and Reverse, 5´-GGAGACGATCTTACGCACTGA-3´) were designed using the Universal
136 ProbeLibrary software (Roche Life Sciences). Results were normalized to the expression level of the
137 endogenous references genes (*TBP*, *HPRT1*) and quantified using the ΔΔCT (cycle threshold)
138 method.

139 **Western blot**. Cell lysates were subjected to SDS-PAGE (50 µg unless indicated otherwise) and
140 transferred onto an Immobilon-P polyvinylidene difluoride membrane (PVDF; Millipore). After

141 blocking the unoccupied sites with 5% non-fat milk diluted in Tris-Buffered Saline plus Tween 20
142 (TBS-T), protein detection was carried out with antibodies against MAFB (HPA005653, Sigma
143 Aldrich), total GSK3α (#4337, Cell Signaling Technology), total GSK3β (#27C10, Cell Signaling
144 Technology), total GSK3 (#5676, Cell Signaling Technology), p-Ser^{9}-GSK3β (#5558, Cell Signaling
145 Technology), p-Ser^{21}-GSK3α (#9316, Cell Signaling Technology), p-Tyr^{279}/P-Tyr^{216}- GSK3α/β (#05-
146 413, Sigma Aldrich), CD163 (#MCA1853, Bio-Rad), MAF (sc-518062, Santa Cruz Biotechnology), IL7R
147 (sc-514445, Santa Cruz Biotechnology) and FOLR2 (clone 94b, kindly provided by Dr. Takami
148 Matsuyama) [39], and vinculin (#V9131, Sigma-Aldrich) or GAPDH (sc-32233, Santa Cruz
149 Biotechnology) as protein loading controls. Quimioluminiscence was detected in a Chemidoc
150 Imaging system (BioRad) using SuperSignal™ West Femto (ThermoFisher Scientific).

151 **RNA-sequencing and data analysis**. RNA isolated from GM-MØ exposed to DMSO or the GSK3β
152 inhibitor CHIR-99021 (10 μM) for 48h, monocytes exposed to CHIR99021 or DMSO, *ex vivo* isolated
153 AMØ exposed to CHIR99021 or DMSO, or GM-MØ transfected with siRNA specific for *GSK3A* and/or
154 *GSK3B*, or a control siRNA, were subjected to sequencing on a BGISEQ-500 platform
155 (https://www.bgitechsolutions.com). RNAseq data were deposited in the Gene Expression Omnibus
156 (http://www.ncbi.nlm.nih.gov/geo/) under accession GSE256538 (monocytes exposed to
157 CHIR99021 or DMSO), GSE256208 (GM-MØ exposed to CHIR99021 or DMSO), GSE262463 (AMØ
158 exposed to CHIR99021 or DMSO) or GSE266236 (GM-MØ transfected with siRNA specific for *GSK3A*,
159 *GSK3B* or a control siRNA). Low quality reads and reads with adaptors or unknown bases were
160 filtered to get the clean reads. Sequences were mapped to GRCh38 genome using HISAT2 [40] or
161 Bowtie2 [41], and clean reads for each gene were calculated using htseq-count [42] and the RSEM
162 software package [43]. Differential gene expression was assessed by using the R-package DESeq2.
163 Differentially expressed genes were analysed for annotated gene sets enrichment using ENRICHR

164 (http://amp.pharm.mssm.edu/Enrichr/) [44,45], and enrichment terms considered significant with a
165 Benjamini-Hochberg-adjusted p value <0.05. For gene set enrichment analysis (GSEA)
166 (http://software.broadinstitute.org/gsea/index.jsp) [46], gene sets available at the website, as well as
167 gene sets generated from publicly available transcriptional studies
168 (https://www.ncbi.nlm.nih.gov/gds), were used. The datasets used throughout the manuscript
169 (either reported here for the first time or previously published) are listed and described in Table S1.
170 **Re-analysis of single cell RNA-seq data.** Single cell RNA-Seq data from 8 healthy lung samples were
171 obtained from GSE128033 [47] and futher analyzed using R programming language. A total of 5898240
172 cells were filtered down to 21310 according to the following criteria: 1) number of genes per cell >
173 200 and < 6000; 2) UMI count > 1000; and 3) mitocondrial genes < 15. Data were then normalized
174 using LogNormalize with a scale factor of 10000 and the top 2000 features were identified with the
175 vst method using Seurat v.5.0.1. The resulting Seurat object was converted into an Anndata object
176 using sceasy v.0.0.7 and the integration was processed using scVI v.1.0.4 and Scanpy v.1.9.8 in a
177 Python enviroment. The trained model was re-converted into a Seurat object. The Seurat
178 FindNeighbors function was used with the scVI reduction to obtain the resulting clusters with a
179 resolution of 1.2. To focus on macrophages and monocytes, macrophage (*CD163*, *FABP4*, *LYVE1* as
180 markers) and monocyte (*FCN1* as marker) clusters were identified and re-integrated using scVI
181 v.1.0.4 in a Python enviroment and later re-clustered in Seurat v.5.0.1 with a resolution of 0.6.
182 **Phagocytosis assay.** Phagocytosis ability was assessed by flow cytometry using pHrodo Red *E. coli*
183 BioParticles Conjugates (Thermo Fisher), following the procedures recommended by the
184 manufacturer. Macrophages were cultured in 24-well plate and exposed to pHrodo bioparticles for
185 60 min at 37 °C/5% CO2. Cells were then harvested and assessed by flow cytometry.
186 **Efferocytosis assay.** Jurkat cells were cultured in RPMI 1640 medium without FCS for 16 h, and then
187 treated with staurosporine (0.5 µg/ml, SIGMA), followed by an incubation at 37 °C for 3 h.

188 Staurosporine treatment yielded a population of 83% annexin V + cells. Apoptotic cells (AC) were
189 resuspended at a concentration of 1×10^6 cells/ml and labeled with CellTrace™ Violet reagent (0.5
190 μM, Invitrogen, Thermo Scientific) for 20 min. For efferocytosis, macrophages were cultured with
191 labeled AC (ratio 1:4) in p24 plates during 1 h at 37 °C. After 1 h, macrophages were rinsed with PBS
192 to remove unbound AC and detached with PBS 5 mM EDTA, and pelleted by centrifugation before
193 analyzing by flow cytometry.

194 **Bioenergetics profile**. The XF24 extracellular flux analyzer (Seahorse Biosciences, North Billerica,
195 MA) was used to determine the bioenergetic profile of intact cells. Briefly, cells were seeded
196 (200,000 cells/well) in XF24 plates (Seahorse Biosciences) and allowed to recover for 24 h. Cells were
197 then incubated in bicarbonate-free DMEM (Sigma-Aldrich) supplemented with 11.11 mM glucose,
198 2 mM L-glutamine, 1 mM pyruvate, and 2% FBS (Sigma-Aldrich) in a CO2-free incubator for 1 h. The
199 oxygen consumption rate (OCR) and extracellular acidification rate (ECAR), a proxy for lactate
200 production, were recorded to assess the mitochondrial respiratory activity and glycolytic activity,
201 respectively. After four measurements under basal conditions, cells were treated sequentially with
202 1 μM oligomycin, 0.6 μM carbonyl cyanide p-(trifluoromethoxy)phenylhydrazone (FCCP), 0.4 μM
203 FCCP, and 0.5 μM rotenone plus 0.5 mM antimycin A (Sigma-Aldrich), with three consecutive
204 determinations under each condition that were subsequently averaged. Nonmitochondrial
205 respiration (OCR value after rotenone plus antimycin A addition) was subtracted from all OCR
206 measurements. ATP turnover was estimated from the difference between the basal and the
207 oligomycin-inhibited respiration, and the maximal respiratory capacity was the rate in the presence
208 of the uncoupler FCCP [48]. Six independent replicas of each analysis were done, and results were
209 normalized according to protein concentration.

210 **Multicolor Fluorescence Confocal Microscopy**

211 Lung samples were collected from autopsies performed on patients who died from diagnosed SARS-
212 CoV-2 infection or unrelated causes (myocardial infarction, as controls) at the Gregorio Marañón
213 Hospital, Madrid. Patient data and samples were obtained in accordance with Ethics Committees of
214 Instituto de Investigación Sanitaria Gregorio Marañón requirements. Formalin-fixed and paraffin-
215 embedded tissues were deparaffinized, rehydrated, and unmasked by steaming in 10 mM sodium
216 citrate buffer pH 9.0 (Dako Glostrup, Denmark) for 7 minutes. Slides were blocked with 5 µg/ml
217 human immunoglobulins solved in blocking serum-free medium (Dako) for 30 minutes, and then
218 sequentially incubated with 5–10 µg/ml primary antibodies, overnight at 4°C, and proper
219 fluorescent secondary antibodies (Jackson Immunoresearch, West Grove, PA, US) for 1h. Washes
220 were performed by immersion in PBS containing 0.05% Tween-20, and single-cell quantification was
221 performed in 3–5 fields imaged with the ACS_APO 20x/NA 0.60 objective of a confocal microscope
222 (Leica, SPE). Mean Fluorescence Intensity (MFI) of proteins of interest was obtained at segmented
223 CD68+ macrophages using the 'analyze particle' plugging of ImageJ2 software [49], as previously
224 shown [50].
225 **Statistical analysis**. Statistical analyses were conducted using the GraphPad Prism software. For
226 comparison of means, and unless otherwise indicated, statistical significance of the generated data
227 was evaluated using the paired Student t test or One-Way ANOVA followed by multiple comparisons
228 using the Dunnett's test or Fisher´s LSD test. In all cases, $p<0.05$ was considered as statistically
229 significant.
230

231 **RESULTS**

232 **Monocyte-derived macrophages generated in the presence of GM-CSF (GM-MØ) or M-CSF (M-**
233 **MØ) differ in the state of activation of GSK3α and GSK3β.** Monocyte-derived M-MØ exhibit a
234 transcriptional profile akin to that of pathogenic macrophages in severe COVID-19 [22], whereas GM-
235 MØ resemble lung alveolar macrophages (AMØ) [22]. Our prior research has established that MAFB
236 determines the transcriptional and functional specification of monocyte-derived M-MØ,
237 characterized by significantly higher MAFB levels compared to GM-MØ [27]. Since the protein levels
238 of large MAF family members (MAF, MAFA, MAFB, NRL) are controlled through GSK3
239 phosphorylation-dependent proteasome degradation [30], we initially assessed the relative levels of
240 the inhibitory (Ser^{21} for GSK3α and Ser^{9} for GSK3β) and activation-associated (Tyr^{279} for GSK3α and
241 Tyr^{216} for GSK3β) phosphorylation of GSK3 in M-MØ and GM-MØ. Ser^{21}-GSK3α and Ser^{9}-GSK3β
242 phosphorylation was more pronounced in M-MØ, aligning with their elevated levels of MAFB (Figure
243 1A). Conversely, no significant difference in Tyr^{279}-GSK3α and Tyr^{216}-GSK3β phosphorylation was
244 observed between M-MØ and GM-MØ (Figure 1B). Therefore, the heightened expression of MAFB
245 in M-MØ correlates with a higher inhibitory phosphorylation of GSK3.

246

247 **Inhibition of GSK3 leads to transcriptional, phenotypic, functional, and metabolic reprogramming**
248 **in monocyte-derived GM-MØ.** Building upon the above findings, we aimed to examine the
249 macrophage re-programming effects of GSK3 activity modulation in GM-MØ through the use of the
250 GSK3 inhibitor CHIR-99021 (Figure 1C). Treatment of GM-MØ with CHIR-99021 for 48 hours resulted
251 in a significant decrease in the activation-associated Tyr^{216}-GSK3β phosphorylation (Figure 1D) and
252 a rapid and robust elevation in MAFB protein levels (Figure 1E; Supplementary Figure 1A).
253 Moreover, reversal of the Tyr^{216}/Ser^{9} GSK3β phosphorylation ratio was also seen after CHIR-99021
254 treatment, albeit it was not observed after exposure to other GSK3 inhibitors (SB-216763 or LiCl;

255 Supplementary Figure 1B). RNA-Seq analysis of CHIR-GM-MØ unveiled a huge transcriptional impact
256 of GSK3 inhibition, with more than 2000 differentially expressed genes ([$\log_2$FC]>1; *adj p* < 0.05)
257 (Figure 1F). Corresponding with the higher MAFB expression, Gene Set Enrichment Analysis (GSEA)
258 showed that the CHIR-GM-MØ transcriptome was significantly enriched in genes that either mark
259 M-MØ (GSE68061) or are upregulated during monocyte-to-M-MØ differentiation (Figure 1G).
260 Conversely, GM-MØ-specific genes (GSE68061) or genes increased during monocyte-to-GM-MØ
261 differentiation, were downregulated (Figure 1G). Additional gene ontology analysis further
262 supported the pathophysiological significance of the macrophage re-programming induced by
263 modulating GSK3 activity. Thus, GSK3 inhibition augmented the expression of the gene sets that
264 define MoMac-VERSE macrophage subsets identified as long-term resident macrophages
265 (Cluster#2) and tumor-associated macrophages with an M2-like signature (Cluster#2, #3, #16, #17)
266 [2] (Figure 1H). Moreover, GSK3 inhibition increased the expression of the gene sets that define
267 pathogenic pro-fibrotic macrophage subsets in severe COVID-19 [(Group 3 or SPP1$^+$, GSE145926) [24],
268 MoAM3 (GSE155249) [25] or CD163$^+$/LGMN$^+$ MØ (EGAS00001005634) [23]] (Figure 1I). Therefore, GSK3
269 inhibition enhances MAFB expression and re-programs macrophage by promoting the acquisition
270 of the gene profile that defines anti-inflammatory and pro-fibrotic macrophages.
271
272 In agreement with the increased MAFB levels detected in CHIR-GM-MØ (Figure 1E), screening for
273 mediators of the re-programming action of GSK3 inhibition using DoRoThEA [51]
274 (https://saezlab.github.io/dorothea/) revealed a significant enrichment in MAFB-regulated genes
275 (Figure 2A), and similar results were yielded upon Enrichr analysis
276 [4544](https://maayanlab.cloud/Enrichr/) (Supplementary Figure 1C). In fact, GSEA confirmed that
277 CHIR-GM-MØ are enriched in MAFB-dependent genes [2227] (Figure 2B-C) along with macrophage
278 genes whose regulatory regions are directly bound by MAFB [52] (75-geneset, Figure 2C), including

279 *CCL2*, *CCL8*, *CCL18*, *IGF1*, *IL10* and *LGMN* (Figure 2D). Importantly, all these changes were reflected
280 in the phenotype of CHIR-GM-MØ, that showed elevated expression of transcription factors like
281 MAF (Figure 2E), cell surface proteins like CD163 and FOLR2 (Figure 2E, F), and soluble factors like
282 CCL2, CCL18, IL-10, LGMN and SPP1 (Figure 2G), all of which are either direct MAFB targets [52] or
283 MAFB-regulated genes [2227]. Likewise, the attenuated expression of the GM-MØ-specific *INHBA* gene
284 (Figure 2D) corresponded to a decrease in Activin A production by CHIR-GM-MØ (Figure 2G). These
285 results underscore the phenotypic re-programming induced by GSK3 inhibition in GM-MØ, wherein
286 there is an upregulation of MAFB-dependent transcription factors, cell surface markers, and soluble
287 factors which collectively define an anti-inflammatory/pro-fibrotic phenotype characteristic of M-
288 CSF-dependent monocyte-derived macrophages.
289
290 Remarkably, the phenotypic changes induced by GSK3 inhibition were also accompanied by
291 alterations in macrophage functional capabilities. Thus, CHIR-GM-MØ exhibited elevated anti-
292 inflammatory activity, evidenced by increased production of IL-10 upon activation by inflammatory
293 cytokines such as TNF or IFNγ, or exposure to PAMPs like LPS or the TLR7 ligand CL264 (Figure 3A).
294 In addition, CHIR-GM-MØ demonstrated increased phagocytic ability for *E. coli* particles (Figure 3B),
295 as well as enhanced efferocytosis (Figure 3C), with both activities being typically higher in M-MØ.
296 Collectively, these findings indicate that GSK3 inhibition re-educates GM-MØ macrophages by
297 facilitating the acquisition of transcriptional, phenotypic, and functional properties characteristic of
298 M-CSF-dependent monocyte-derived macrophages. Of note, in line with the well-established
299 connection between inflammatory potential and metabolic state in macrophages [53], GSK3 inhibition
300 also induced modifications in various metabolic parameters in GM-MØ, including basal respiration
301 and maximal ATP production (Supplementary Figure 1D-F).
302

303 **siRNA-mediated knock-down of *GSK3A* and/or *GSK3B* enhances the expression of the MAFB-**
304 **dependent profiles of M-MØ and pathogenic pro-fibrotic lung macrophages.** To fully support the
305 involvement of GSK3 in the macrophage re-programming action of CHIR-99021, we next assessed
306 the transcriptional consequences of knocking-down *GSK3A* (coding for GSK3α) and/or *GSK3B*
307 (coding for GSK3β) in GM-MØ (Figure 4A,B). Like CHIR-99021, silencing of both *GSK3A* and *GSK3B*
308 augmented the expression of MAFB (Figure 4B), and modulated the expression of 329 genes, with
309 the simultaneous silencing of both *GSK3A* and *GSK3B* genes having a stronger effect (Figure 4C,D).
310 Of note, silencing of *GSK3A* and *GSK3B* reproduced the effects of CHIR-99021, as it strongly
311 enhanced the expression of genes upregulated by the inhibitor in either GM-MØ or *ex vivo* isolated
312 Alveolar Macrophages (Figure 4E and not shown). *GSK3A/B* knock-down triggered a significant
313 enrichment in the expression of MAFB-dependent genes (Figure 4F), genes acquired along the
314 monocyte-to-M-MØ differentiation (Figure 4G), and genes that mark M-MØ, while reducing the
315 expression of GM-MØ-specific genes (Figure 4G). Furthermore, in agreement with the effect of
316 CHIR-99021, *GSK3A/B* knock-down enhanced the expression of the MoMac-VERSE macrophage
317 subsets Cluster#2 and Cluster#3 [2] (Figure 4H) as well as the gene sets that define pathogenic pro-
318 fibrotic macrophage subsets in severe COVID-19 [(SPP1$^+$, GSE145926) [24], MoAM3 (GSE155249) [25] or
319 CD163$^+$/LGMN$^+$ MØ (EGAS00001005634) [23]] (Figure 4I, Supplementary Figure 2A). Conversely,
320 silencing of *GSK3A* and *GSK3B* drastically reduced the expression of the gene sets that characterize
321 tissue-resident lung Alveolar Macrophages in COVID-19, with the concomitant silencing of *GSK3A*
322 and *GSK3B* again showing a stronger effect (Figure 4I). Altogether, these results support the
323 relevance of GSK3α and GSK3β as relevant targets for human macrophage re-programming.
324
325 **GSK3 inhibition redirects monocytes towards acquiring a gene profile reminiscent of anti-**
326 **inflammatory M-MØ.** Given the swift and profound anti-inflammatory impact observed in fully

327 differentiated GM-MØ upon GSK3 inhibition or knock-down, we next delved into assessing whether
328 modulation of GSK3 activity influence the differentiation capability of peripheral blood monocytes.
329 To that end, monocytes were exposed to CHIR-99021, and the resulting cells (CHIR-Mon, Figure 5A)
330 exhibited increased MAFB levels as early as 16 hours post-treatment (Figure 5B). Remarkably, the
331 16-hour exposure to the GSK3 inhibitor induced significant alterations in the expression of over 2000
332 genes ([$\log_2$FC]>1; *adj p* < 0.05) (Figure 5C) and sufficed to augment the expression of M-MØ-specific
333 genes and genes upregulated during M-CSF-dependent monocyte-to-M-MØ differentiation (Figure
334 5D), including *CCL2*, *CD163* and *IL10* (Figure 5E). Notably, the transcriptome of CHIR-Mon exhibited
335 a significant enrichment in MAFB-dependent genes (Figure 5F, Supplementary Figure 2B) and genes
336 characterizing the MAFB+ pathogenic macrophages in severe COVID-19 (Supplementary Figure 2C),
337 whereas it showed an under-representation of genes inhibited by MAFB (22)(27)[52] (Figure 5F).
338 Compared to DMSO, CHIR-99021 treatment upregulated the expression of 25% of M-MØ-specific
339 genes, including MAFB-dependent genes like *CCL2*, *IL10* and *CD163*, while downregulating 30% of
340 GM-MØ-specific genes (Figure 5G), and this transcriptional effect was also evident in comparison
341 with M-CSF-treated monocytes (Supplementary Figure 2D). To broaden the scope of these findings,
342 we also examined the consequences of inhibiting GSK3 in monocytes exposed to a pathologic pro-
343 inflammatory environment, namely synovial fluid from patients with active rheumatoid arthritis
344 (RASF) (Figure 5H). Evaluation of CHIR-99021-treated monocytes in the presence of RASF revealed
345 an enhanced expression of MAFB (Figure 5I) and MAFB-dependent genes such as *IL10* and *LGMN*
346 (Figure 5J). Therefore, GSK3 inhibition in monocytes also leads to heightened MAFB expression,
347 ultimately steering differentiation towards anti-inflammatory monocyte-derived macrophages.
348
349 **Inhibition of GSK3 in *ex vivo* isolated human alveolar macrophages promotes the acquisition of**
350 **an M-MØ-like anti-inflammatory profile.** To further validate the macrophage re-programming

351 potential of GSK3 inhibition, we next conducted experiments on *ex vivo* isolated human alveolar
352 macrophages (AMØ, Figure 6A), whose development and gene expression profile is GM-CSF-
353 dependent [17,18,19]. To that end, we determined the transcriptome of three independent isolates of
354 AMØ, purified from broncho-alveolar lavages, after exposure to CHIR-99021 for 24 hours (Figure
355 6A). A total of 865 differentially expressed genes ([$\log_2$FC]>1; *adj p* < 0.05) were identified, with 316
356 genes upregulated in CHIR-AMØ (Figure 6B). Further comparisons and gene ontology analysis
357 revealed that GSK3 inhibition by CHIR-99021 (CHIR-AMØ) upregulated the gene sets that define
358 pathogenic pro-fibrotic macrophage subsets in severe COVID-19 [(SPP1$^+$, GSE145926) [24], MoAM3
359 (GSE155249) [25] or CD163$^+$/LGMN$^+$ MØ (EGAS00001005634) [23]] (Figure 6C,D; Supplementary Figure
360 2E). Conversely, CHIR-AMØ exhibited a reduced expression of the gene sets that characterize lung-
361 resident AMØ in severe COVID-19 [AMØ1+AMØ2 clusters from EGAS00001005634) [23], FABP4+ from
362 GSE145926) [24], TRAM1 from GSE155249 [25]] (Figure 6D,E; Supplementary Figure 2F), including key
363 AMØ-specific genes like *FABP4* and *MARCO* (Figure 6E), and similar resuts were seen upon analysis
364 of AMØ-specific gene sets from other studies [25,54] (Supplementary Figure 2F). Like in the case of
365 CHIR-GM-MØ, CHIR-AMØ exhibited an over-representation of M-MØ-specific genes and genes
366 acquired along the monocyte-to-M-MØ differentiation (GSE188278) (Supplementary Figure 2G).
367 Consistent with these findings, CHIR-AMØ exhibited higher expression of MAFB (Figure 6F) whose
368 increase correlated with an augmented secretion of Legumain, IL-10 and CCL2 (Figure 6G). In
369 contrast, lower levels of activin A were detected in CHIR-AMØ-conditioned medium (Figure 6G).
370 Remarkably, and in agreement with the shift in macrophage subsets that takes place in severe
371 COVID-19 lungs (loss of AMØ, appearance of monocyte-derived pro-fibrotic macrophages) [22,23–25],
372 the level of phosphorylated Ser^{21}-GSK3α and Ser^{9}-GSK3β was very significantly augmented in lung
373 macrophages (CD68+) from severe COVID-19 patients, an increase that correlated with a robust
374 enhancement of the macrophage expression of both MAFB and the MAFB-dependent protein

375 CD163 (Figure 6H). These results collectively demonstrate that macrophage re-programming
376 through GSK3 inhibition can also be achieved on *in vivo* isolated macrophages, leading to enhanced
377 expression of MAFB and MAFB-dependent genes, the acquisition of an anti-inflammatory
378 transcriptional profile and the loss of the signature of lung-resident human AMØ.
379
380 **GSK3- and MAFB-dependent genes are differentially expressed between human lung alveolar and**
381 **interstitial macrophages.** To assess whether GSK3 inhibition also modulates the phenotypic
382 differences between human lung macrophage subsets in a physiological setting, we next took
383 advantage of the available information on human healthy lungs obtained by single cell-RNA
384 sequencing [47]. Re-analysis of the single cell-RNA sequencing data [47] (Figure 7A; Supplementary
385 Figure 3A) revealed several clusters expressing macrophage-associated markers (*CD163*, *FABP4*,
386 *LYVE1, FCN1*) (Supplementary Figure 3B), and whose subsequent re-clustering identified cell subsets
387 expressing previously defined markers for infiltrating monocytes (Cluster 4/7/12:*FCN1*) [23], Alveolar
388 macrophages (AMØ) (Clusters 0/2/5/13: *FABP4 TYMS*-negative*;* Cluster 9*: MARCO*, *INHBA; Cluster*
389 *11: PPARG*), proliferating AMØ (Cluster 15: *TYMS, MKI67, TOP2A, NUSAP1*) [23], and Interstitial
390 Macrophages (IMØ) that variably express markers for tissue-resident macrophages like *LYVE1,*
391 *RNASE1* and *LGMN* (Clusters 1/3/6/8/10/14) [14723] (Figure 7B; Supplementary Figure 3C). The
392 comparison of IMØ and AMØ subsets revealed that the genes upregulated upon inhibition of GSK3
393 include numerous MAFB-dependent genes (e.g., *MAFB*, *IL10*, *LGMN*, *SPP1*, *CCL2*) and showed a
394 higher expression in IMØ (Figure 7C). On the other hand, the genes downregulated by CHIR-99021
395 were preferentially or exclusively expressed in AMØ, including *INHBA*, *GSN*, *FBP1*, *PPARG*, *AXL* and
396 *AQP3* (Figure 7C). Therefore, GSK3 inhibition prompts macrophages towards the acquisition of a
397 gene profile that resembles that of IMØ, while provokes the loss of the AMØ gene signature. Such
398 a conclusion was also reached upon analysis of pseudo bulk-RNA sequencing data from GSE128033

399 [47]. Indeed, numerous MAFB-dependent and GSK3-regulated genes were found within the 712 genes
400 that are differentially expressed ([$\log_2$FC]>1; *adj p* < 0.05) between IMØ and AMØ (Figure 7D).
401 Further GSEA evidenced that GSK3 inhibition in either GM-MØ (CHIR-GM-MØ) (Figure 7E) or AMØ
402 (CHIR-AMØ) (Figure 7F) very significantly enhance the expression of MAFB-dependent IMØ-specific
403 genes (as defined by Morse *et al*. [47] or by Li *et al*. [55]), while simultaneosuly impaired the expression
404 of genes characterizing human AMØ (Figure 7E-F). More importantly, a similar effect was observed
405 after *GSK3A/B* silencing in GM-MØ, that yielded an enhanced expression of IMØ-specific genes and
406 a downregulation of the gene set that defines AMØ (Figure 7G). Altogether, these results indicate
407 that inhibiting GSK3 shifts the gene profile of Alveolar Macrophages towards that of Interstitial
408 Macrophages (or monocyte-derived macrophages), and imply that the activation status of GSK3
409 significantly influences the specification of lung-resident macrophages (AMØ *vs*. IMØ).

410 **DISCUSSION**

411 Our previous investigations have demonstrated that the macrophage re-programming effect of LXR
412 modulators [5638] and methotrexate [37] coincide with alterations in the protein levels of MAFB.
413 Similarly, intravenous immunoglobulins have been shown to alter the inflammatory state of
414 macrophages and modulate MAFB levels [57]. Building upon these findings and others, we have
415 explored whether modulating the activity of GSK3, a primary regulator of MAFB protein levels and
416 activity, is sufficient to induce a shift in the inflammatory profile of human macrophages. Our results
417 indicate that GSK3 inhibition impairs the expression of genes associated with GM-CSF-dependent
418 differentiation of monocyte-derived macrophages while concurrently promoting the acquisition of
419 genes and functions associated with M-CSF-dependent monocyte-derived macrophages,
420 particularly those regulated by MAFB. The physiological relevance of these findings is underscored
421 by the contrasting effect that GSK3 inhibition has on genes that define lung-resident alveolar
422 macrophages (decrease) versus monocyte-derived macrophages recruited into the lung (increase)
423 during inflammatory responses. Thus, modulation of GSK3 activity emerges as a plausible strategy
424 for macrophage reprogramming in therapeutic interventions.

425

426 Therapeutic approaches aimed at re-educating tumor-associated macrophages into
427 immunostimulatory cells [58] may involve targeting the macrophage PI3Kγ intracellular signaling
428 pathway [59], which inhibits NFκB activation through Akt and mTOR [60], thereby inducing an anti-
429 inflammatory program that promotes immune suppression. Indeed, macrophage PI3Kγ inactivation
430 stimulates and prolongs NFκB activation, promoting an immunostimulatory transcriptional program
431 [60]. The ability of PI3Kγ to toggle between immune stimulation and suppression aligns with our
432 findings on GSK3 inhibition, as PI3Kγ inactivates GSK3 via phosphorylation of Ser^{9} (GSK3β) and Ser^{21}
433 (GSK3α) [30]. Threfore, GSK3 inhibition may contribute to the anti-inflammatory and

434 immunosuppressive effects of PI3Kγ inactivation by enhancing MAFB expression. Moreover, MAFB
435 might even participate in the macrophage reprogramming consequences of mTOR modulation [616263]
436 due to the known reciprocal interactions between GSK3 and mTOR [64]. Hence, since the
437 phosporylation of MAFB by GSK3 requires of a prior "priming" phosphorylation event [30],
438 identification of the MAFB priming kinase(s) emerges as a potentially relevant effort in the search
439 for additional targets for macrophage re-programming.
440
441 The significant impact of GSK3 inhibition by CHIR-99021 on the macrophage transcriptional profile
442 mirrors the effects observed with other GSK3 inhibitors on the differentiation of monocyte-derived
443 dendritic cells (MDDC) [65]. Specifically, GSK3 inhibitors like LiCl, SB415286, or SB216763 redirect the
444 GM-CSF+IL-4-dependent development of MDDC towards the generation of macrophage-like cells [65].
445 Considering that MAFB expression is higher in monocyte-derived macrophages than in dendritic
446 cells [66], it is reasonable to infer that GSK3 inhibitors also boost MAFB expression in cells
447 differentiated in the presence of GM-CSF+IL-4, thereby supporting the modulation of GSK3 activity
448 as a tool to alter lineage determination in myeloid cells.
449
450 The re-programming effect of GSK3 inhibition on *ex vivo* isolated alveolar macrophages bears
451 significant therapeutic implications, particularly in severe COVID-19 cases where profibrotic
452 monocyte-derived macrophages replace GM-CSF-dependent tissue-resident alveolar macrophages
453 [672324]. Our observations reveal that exposure of *ex vivo* isolated alveolar macrophages to CHIR-99021
454 leads to the loss of the alveolar macrophage GM-CSF-dependent gene profile and the acquisition of
455 a MAFB-dependent pro-fibrotic transcriptional landscape resembling that of M-CSF-dependent
456 monocyte-derived macrophages. Given that MAFB serves as a negative regulator of GM-CSF
457 signaling [68], downregulation of MAFB expression through modulation of GSK3 activity emerges as a

458 rationale strategy to re-direct pathogenic monocyte-derived macrophages towards the acquisition
459 of a lung-resident alveolar macrophage-like profile during severe COVID-19. This approach aligns
460 with the proposed therapeutic use of GM-CSF in COVID-19 [69,70], as GM-CSF would impede or limit
461 the MAFB-dependent upregulation of profibrotic and neutrophil-attracting factors observed in
462 severe COVID-19 [52].

ACKNOWLEDGEMENTS

This work was supported by grant PID2020-114323RB-I00 from Ministerio de Ciencia e Innovación to ALC, Dirección General de Innovación e Investigación Tecnológica de la Comunidad de Madrid (RETARACOVID, P2022/BMD-7274) to ALC, APK, PS-M and RD, Instituto de Salud Carlos III (Grant PI23/00224 to APK, Grant PI21/00989 to RD), Red de Enfermedades Inflamatorias (RICORS RD21/0002/0034) from Instituto de Salud Carlos III and cofinanced by the European Regional Development Fund "A way to achieve Europe" (ERDF) and PRTR to APK, and PID2021-123167OB-I00 from Ministerio de Ciencia, Innovación y Universidades and CSIC Talent Attraction program (20222AT010) to EO. This research work was also funded by the European Commission – NextGenerationEU (Regulation EU 2020/2094), through CSIC's Global Health Platform (PTI Salud Global). AN-V was funded by YEI program contract from Comunidad de Madrid (PEJ-2021-AI/BMD-23327). IR was funded by a Formación de Personal Investigador predoctoral fellowship from Ministerio de Ciencia e Innovación (Grant PRE2021-097080). Figures were created with Biorender.com.

AUTHORSHIP CONTRIBUTIONS

IR, CH, MT-T, BL-N, MT-S, FD-C, AN-V, RS and YS-P performed research and analyzed data; EO, PS-M, RD, AP-K and ALC designed research and analyzed data; FR-S and RG-L identified suitable patients for broncho-alveolar lavage; IR, APK and ALC wrote the paper.

DISCLOSURE OF CONFLICTS OF INTEREST

The authors declare no competing financial interests.

AVAILABILITY OF DATA AND MATERIALS

487 The dataset supporting the conclusions of this article is available in the Gene Expression Omnibus
488 repository (http://www.ncbi.nlm.nih.gov/geo/) under accession GSE256538 (monocytes exposed to
489 CHIR99021 or DMSO), GSE256208 (GM-MØ exposed to CHIR99021 or DMSO), GSE262463 (alveolar
490 macrophages exposed to CHIR99021 or DMSO) and GSE266236 (GM-MØ after GSK3α/β
491 knockdown).

492 **FIGURE LEGENDS**

493 **Figure 1. Transcriptional effect of GSK3 inhibition on monocyte-derived GM-MØ. A**. MAFB, total
494 GSK3α, total GSK3β, Ser^{9}-phosphorylated GSK3β and Ser^{21}-phosphorylated GSK3α levels in M-MØ
495 and GM-MØ, as determined by Western blot (left panel). GAPDH protein levels were determined as
496 protein loading control. Mean ± SEM of the MAFB/GAPDH, Ser^{21}-phosphorylated GSK3α/total
497 GSK3α and Ser^{9}-phosphorylated GSK3β/total GSK3β protein ratios from three independent
498 experiments are shown (right panel) (***, p<0.005; ****, p<0.001). A representative Western blot
499 experiment is shown in each case in the upper panel. **B**. p-Tyr^{279}-GSK3α and p-Tyr^{216}-GSK3β levels
500 in four independent samples of M-MØ and GM-MØ, as determined by Western blot (left panel).
501 GAPDH protein levels were determined as protein loading control. Mean ± SEM of the p-Tyr^{279}-
502 GSK3α/GAPDH and p-Tyr^{216}-GSK3β/GAPDH protein ratios from four independent experiments are
503 shown (right panel). **C.** Schematic representation of the exposure of GM-MØ to CHIR-99021 for 48
504 hours. **D.** Tyr^{279}-phosphorylated GSK3α and Tyr^{216}-phosphorylated GSK3β levels in three
505 independent preparations of DMSO- or CHIR-99021-treated GM-MØ, as determined by Western
506 blot (left panel). GAPDH protein levels were determined as protein loading control. Mean ± SEM of
507 the p-Tyr^{216}-GSK3β/GAPDH and p-Tyr^{279}-GSK3α/GAPDH protein ratios from the three independent
508 experiments are shown (right panel) (****, p<0.001). **E**. MAFB protein levels in DMSO-GM-MØ and
509 CHIR-GM-MØ, as determined by Western blot. A representative experiment is shown. **F**. Number of
510 differentially expressed genes ([log2FC] >1; adjp<0.05) between DMSO-GM-MØ and CHIR-GM-MØ.
511 **G**. GSEA of the indicated gene sets (from GSE68061, left panel; from GSE188278, right panel) on the
512 ranked comparison of the CHIR-GM-MØ vs. DMSO-GM-MØ transcriptomes. Normalized Enrichment
513 Score (NES) and FDRq values are indicated in each case. **H**. Summary of GSEA of the gene sets that
514 define the tissue-resident monocyte and macrophage states (MoMac-VERSE) [2] on the ranked

515 comparison of the CHIR-GM-MØ vs. DMSO-GM-MØ transcriptomes. FDRq values are indicated only
516 if FDRq>0.0; empty dots, Not Significant. **I.** Summary of GSEA of the gene sets that characterize the
517 macrophage subsets identified in severe COVID-19 [232524] on the ranked comparison of the CHIR-GM-
518 MØ vs. DMSO-GM-MØ transcriptomes. FDRq values are indicated only if FDRq>0.0; empty dots, Not
519 Significant.

520

521 **Figure 2.- Phenotypic effects of GSK3 inhibition on monocyte-derived GM-MØ: Enhanced**
522 **expression of MAFB-dependent genes and proteins. A.** DoRoThEA [51] analysis on the ranked
523 comparison of the DMSO-GM-MØ and CHIR-GM-MØ transcriptomes. **B**. GSEA of MAFB-regulated
524 gene sets (from GSE155719) on the ranked comparison of the DMSO-GM-MØ and CHIR-GM-MØ
525 transcriptomes. NES and FDRq values are indicated in each case **C**. Overlap between the genes
526 upregulated (|log2FC|>1; adjp<0.05) in CHIR-GM-MØ (relative to DMSO M-MØ) and MAFB-
527 dependent genes (from GSE155719, left panel) or the 75-geneset of MAFB-regulated genes (right
528 panel) [52], with indication of some of the overlapping genes. **D**. Relative mRNA levels of the indicated
529 genes in DMSO-GM-MØ and CHIR-GM-MØ, as determined by RNA-Seq on three independent
530 samples (GSE256208). *Adjp* of the comparison is shown in each case. **E**. CD163, MAF and IL7R protein
531 levels in DMSO-GM-MØ and CHIR-GM-MØ, as determined by Western blot (left panel). GAPDH
532 protein levels were determined as protein loading control. Mean ± SEM of the MAF/GAPDH,
533 IL7R/GAPDH and CD163/GAPDH protein ratios from seven independent experiments are shown
534 (right panels) (***, p<0.005; ****, p<0.001). A representative Western blot experiment is shown in
535 each case. **F**. FOLR2 protein levels in DMSO-GM-MØ and CHIR-GM-MØ, as determined by Western
536 blot (left panel). Vinculin protein levels were determined as protein loading control. Mean ± SEM of
537 the FOLR2/Vinculin protein ratio from three independent experiments are shown (lower panel) (**,
538 p<0.01). A representative Western blot experiment is shown. **G**. Production of the indicated soluble

539 factors by DMSO-GM-MØ and CHIR-GM-MØ, as determined by ELISA. Mean ± SEM of seven
540 independent samples are shown (*, p<0.05; **, p<0.01; ***, p<0.005; ****, p<0.001).
541
542 **Figure 3.- Functional consequences of GSK3 inhibition on monocyte-derived GM-MØ. A.**
543 Production of IL-10 by untreated (-) or stimulated (LPS, TNF, IFNγ or CL264) DMSO-GM-MØ and
544 CHIR-GM-MØ, as determined by ELISA. Mean ± SEM of four independent samples are shown (*,
545 p<0.05; **, p<0.01; ***, p<0.005; ****, p<0.001). **B.** Phagocytosis of pHRodo-labeled bacterial
546 particles by DMSO-GM-MØ and CHIR-GM-MØ, as determined by flow cytometry. Mean ± SEM of
547 three independent samples are shown (*, p<0.05). A representative flow cytometry analysis is
548 shown in the left panel. **C**. Efferocytosis capacity of DMSO-GM-MØ, CHIR-GM-MØ and DMSO-M-
549 MØ, as determined by flow cytometry using staurosporine-induced CellTrace Violet-labeled
550 apoptotic Jurkat cells. The percentage of positive cells and mean fluorescence intensity are shown.
551 Mean ± SEM of 3 independent samples are shown (*, p<0.05; **, p < 0.01; ***, p < 0.005).
552 Representative flow cytometry histograms for CellTrace Violet emission of DMSO-GM-MØ, CHIR-
553 GM-MØ and DMSO-M-MØ are shown.
554
555 **Figure 4.- Transcriptional effects of GSK3 knock-down in monocyte-derived GM-MØ. A.** Schematic
556 representation of the siRNA-mediated GSK3 knock-down procedure in monocyte-derived GM-MØ.
557 **B**. Total GSK3α, GSK3β and MAFB protein levels in monocyte-derived GM-MØ after siRNA-mediated
558 *GSK3A* and/or *GSK3B* silencing, as determined by Western blot (upper panel). GAPDH protein levels
559 were determined as protein loading control. Mean ± SEM of GSK3β/GAPDH and GSK3α/GAPDH
560 protein ratios from the three independent experiments are shown (lower panel) (*, p<0.05). **C**.
561 Heatmap of the relative expression of the genes significantly altered after *GSK3A* and *GSK3B* knock-
562 down in siCNT-GM-MØ (lanes A-C), siGSK3A-GM-MØ (lanes D-F), siGSK3B-GM-MØ (lanes G-I),

563 siGSK3A/B-GM-MØ (lanes J-L). Representative genes are indicated. **D**. Number of differentially
564 expressed genes (adjp<0.05) between siGSK3A-GM-MØ, siGSK3B-GM-MØ or siGSK3A/B-GM-MØ
565 and siCNT-GM-MØ. **E**. GSEA of the genes whose expression is significantly modulated by CHIR-99021
566 in either GM-MØ (from Figure 1, this manuscript) or in *ex vivo* isolated Alveolar Macrophages (AMØ,
567 see below in Figure 6) on the ranked comparison of the siGSK3A/B-GM-MØ vs. siCNT-GM-MØ
568 transcriptomes. **F.** GSEA of the indicated gene sets (from GSE68061) on the ranked comparison of
569 the siGSK3A/B-GM-MØ vs. siCNT-GM-MØ transcriptomes. **G**. Summary of GSEA of the indicated
570 gene sets (from GSE188278) on the ranked comparison of siGSK3A/B-GM-MØ vs. siCNT-GM-MØ. **H.**
571 Summary of GSEA of the gene sets that define the tissue-resident monocyte and macrophage states
572 (MoMac-VERSE) [2] on the ranked comparison of the siGSK3A/B-GM-MØ vs. siCNT-GM-MØ
573 transcriptomes. FDRq values are indicated only if FDRq>0.0; empty dots, Not Significant. **I.** Summary
574 of GSEA of the gene sets that characterize the macrophage subsets identified in severe COVID-19
575 [232524] on the ranked comparison of siGSK3A/B-GM-MØ vs. siCNT-GM-MØ. FDRq values are indicated
576 only if FDRq>0.0; empty dots, Not Significant.
577
578 **Figure 5.- Transcriptional effects of GSK3 inhibition on human peripheral blood monocytes. A.**
579 Schematic representation of the exposure of human monocytes to CHIR-99021 or DMSO for 16h. **B**.
580 MAFB protein levels in monocytes exposed for 16h to DMSO, CHIR-99021 or M-CSF, as determined
581 by Western blot (left panel). Vinculin protein levels were determined as protein loading control.
582 Mean ± SEM of the MAFB/Vinculin protein ratio from the three independent experiments shown
583 (right panel) (***, p<0.005). **C**. Number of differentially expressed genes ([log2FC] >1; adjp<0.05)
584 between DMSO-Mon and CHIR-Mon. **D**. GSEA of the indicated gene sets (from GSE68061, upper
585 panel; from GSE188278, lower panel) on the ranked comparison of the DMSO-Mon and CHIR-Mon
586 transcriptomes. NES and FDRq values are indicated in each case. **E**. Relative mRNA levels of the

587 indicated genes in monocytes exposed for 16h to DMSO, CHIR-99021 or M-CSF, as determined by
588 RNA-Seq on three independent samples (GSE256538). *Adjp* of the comparison is shown in each case.
589 **F**. GSEA of MAFB-regulated gene sets (from GSE155719) on the ranked comparison of the DMSO-
590 Mon and CHIR-Mon transcriptomes. NES and FDRq values are indicated in each case. **G**. Overlap
591 between the genes upregulated (|log2FC|>1; adjp<0.05) in CHIR-Mon (relative to DMSO-Mon) and
592 M-MØ-specific marker genes (from GSE68061) (left panel) and genes downregulated (|log2FC|>1;
593 adjp<0.05) in CHIR-Mon (relative to DMSO-Mon) and GM-MØ-specific marker genes (from
594 GSE68061) (right panel), with indication of some of the overlapping genes. **H**. Schematic
595 representation of the exposure of human monocytes to synovial fluid from rheumatoid arthritis
596 patients (RASF) for 48h in the presence or absence of CHIR-99021. **I**. MAFB protein levels in
597 monocytes exposed to three independent samples of RASF in the presence of DMSO or CHIR-99021,
598 as determined by Western blot (upper panel). Vinculin protein levels were determined as protein
599 loading control. Mean ± SEM of the MAFB/Vinculin protein ratio from seven independent
600 experiments using three monocyte preparations and three unrelated RASF (lower panel) (**,
601 p<0.01). **J**. Relative expression of *IL10* and *LGMN* in monocytes exposed to RASF in the presence of
602 DMSO or CHIR-99021, as determined by RT-PCR. Mean ± SEM of the results from the three
603 independent samples are shown (**, p<0.01).
604
605 **Figure 6.- Transcriptional and phenotypic effects of GSK3 inhibition on *ex vivo* isolated human**
606 **alveolar macrophages. A**. Schematic representation of the exposure of *ex vivo* isolated human
607 alveolar macrophages to CHIR-99021 or DMSO for 24h. **B**. Volcano plot depicting the differentially
608 expressed genes between CHIR-AMØ and DMSO-AMØ. **C**. Heatmap of the relative expression of the
609 genes within the CD163+/LGMN+ pro-fibrotic monocyte-derived macrophage cluster (from
610 EGAS00001005634) [23] in DMSO-AMØ (lanes A-C) and CHIR-AMØ (lanes D-F). Differentially expressed

611 between CHIR-AMØ and DMSO-AMØ are shown in greeen, and MAFB-dependent genes
612 (GSE155719) are shown in blue. Representative genes are indicated. **D**. (Upper panel) GSEA of the
613 gene sets that characterize the monocyte-derived profibrotic macrophage subsets identified in
614 severe COVID-19, namely CD163+/LGMN+ (EGAS00001005634) [23], MoAM3 (GSE155249) [25] and
615 SPP1+ (GSE145926) [24], on the ranked comparison of the transcriptomes of CHIR-AMØ vs. DMSO-
616 AMØ. NES and FDRq values are indicated in each case. (Lower panel) GSEA of the gene sets that
617 characterize tissue-resident alveolar macrophages in severe COVID-19, namely AMØ1
618 (EGAS00001005634) [23], TRAM1+ (GSE155249) [25] and FABP4+ (GSE145926) [24], on the ranked
619 comparison of the transcriptomes of CHIR-AMØ vs. DMSO-AMØ. **E.** Heatmap of the relative
620 expression of the genes within the Alveolar Macrophage signature (including all the genes
621 overexpressed in the AMØ1 and AMØ2 macrophages clusters from EGAS00001005634) [23] in DMSO-
622 AMØ (lanes A-C) and CHIR-AMØ (lanes D-F). Differentially expressed between CHIR-AMØ and
623 DMSO-AMØ are indicated in greeen, and selected genes are shown. **F**. MAFB protein levels in three
624 independent samples of *ex vivo* isolated AMØ exposed to DMSO or CHIR-99021 for 24h, as
625 determined by Western blot. GAPDH protein levels were determined as protein loading control. **G**.
626 Production of the indicated soluble factors by three independent preparations of DMSO-AMØ and
627 CHIR-AMØ, as determined by ELISA. **H**. Expression of inactive GSK3 (S9, $pSer^{9}$-GSK3β; S21, $pSer^{21}$-
628 GSK3α), MAFB and CD163 in human lung macrophages. Representative human lung tissues from
629 COVID (n= 2) and control (n= 3) patients co-stained for CD68 (macrophage marker, red), Ser^{21}-
630 phosphorylated GSK3α, Ser^{9}-phosphorylated GSK3β, MAFB or CD163 (green), and DAPI (nuclei,
631 blue), as indicated. Plots show MFI (in arbitrary units, a.u.) of single-cell CD68+ macrophages stained
632 for each antibody. Scale bar, 50 µm.
633

634 **Figure 7**. **Differential expression of GSK3-regulated genes in human lung interstitial and alveolar**
635 **macrophages. A**. UMAP (Uniform Manifold Approximation and Projection) embedding of 5898240
636 single-cell transcriptomes from human lungs. Cell-type annotation is based on expression of
637 canonical marker genes, as reported in [47]. **B**. Two-dimensional embedding computed by UMAP on
638 21310 computationally identified macrophages after filtering according to 1) number of genes per
639 cell > 200 and < 6000; 2) UMI count > 1000; and 3) mitocondrial genes < 15. **C**. Relative expression
640 of the indicated genes in the four macrophage subsets defined upon re-clustering of the 21310
641 macrophages identified in the single cell RNA sequencing reported in GSE128033 [47]. **D**. Volcano plot
642 illustrating the differentially expressed genes between the Interstitial Macrophage (IMØ) and
643 Alveolar Macrophage (AMØ) subsets defined upon re-analysis of the single cell RNA sequencing
644 reported in GSE128033 [47]. **E-G**. GSEA of the gene sets that define human lung AMØ or IMØ
645 macrophage subsets (GSE128033 and GSE193782) [47,55] on the ranked comparison of CHIR-GM-MØ
646 vs. DMSO-GM-MØ transcriptomes (**E**), CHIR-AMØ vs. DMSO-AMØ transcriptomes (**F**) or siGSK3A/B-
647 GM-MØ vs. siCNT-GM-MØ (**G**).
648
649 **SUPPLEMENTARY FIGURE LEGENDS**
650 **Figure S1.- A**. MAFB protein levels in GM-MØ exposed to DMSO or CHIR-99021 for 4-8 hours, as
651 determined by Western blot (left panel). GAPDH protein levels were determined as protein loading
652 control. Mean ± SEM of the MAFB/GAPDH protein ratio from three independent experiments are
653 shown (right panel) (*, p<0.05; **, p<0.01). **B**. p-Ser^{9}-GSK3β and p-Tyr^{216}-GSK3β levels in GM-MØ
654 treated with DMSO, CHIR-99021 (10 μM), SB-216763 (10 μM) or LiCl (10 mM) for 48 hours, as
655 determined by Western blot. A representative experiment of three independent experiments is
656 shown in the left panel. GAPDH protein levels were determined as protein loading control. **C**. Gene
657 ontology analysis of the genes upregulated (|log2FC|>1; adjp<0.05) in CHIR-GM-MØ (relative to

658 DMSO GM-MØ) using Enrichr and the indicated databases. **D**. Oxygen Consumption rate (OCR)
659 profile of DMSO-GM-MØ and CHIR-GM-MØ monitored using the Seahorse Biosciences extracellular
660 flux analyzer at the indicated time points. Cells were treated sequentially, as indicated, with 1 mM
661 oligomycin (Oligo), 0.6 plus 0.4 mM FCCP, and 1 mM rotenone plus 1 mM antimycin A (Rot/AA). **E**.
662 Extracellular acidification rate (ECAR), a proxy for the rate of lactate production, measured in DMSO-
663 GM-MØ and CHIR-GM-MØ under basal conditions and after the stimulation with 1 mM oligomycin
664 and at the indicated time points. **F**. Metabolic parameters obtained from the OCR and ECAR profiling
665 after subtraction of the rotenone/antimycin-insensitive respiration. Basal OCR is the oxygen
666 consumption rate in the absence of effectors, ATP turnover is considered as the oligomycin-sensitive
667 respiration, maximal respiration is the OCR value in the presence of the uncoupler FCCP, glycolytic
668 capacity is the ECAR value after the inhibition with oligomycin of the mitochondrial ATP synthesis.
669 In **D-F**, results are normalized according to protein concentrations and presented as mean ± SEM of
670 six independent samples.
671
672 **Figure S2. A**. Summary of GSEA of the gene sets that characterize the macrophage subsets identified
673 in severe COVID-19 [232524] on the ranked comparison of siGSK3A-GM-MØ vs. siCNT-GM-MØ (square
674 symbols), siGSK3B-GM-MØ vs. siCNT-GM-MØ (star symbols) and siGSK3A/B-GM-MØ vs. siCNT-GM-
675 MØ. FDRq values are indicated only if FDRq>0.0; empty dots, Not Significant. **B.** GSEA of *bona fide*
676 MAFB-bound genes ("75-genelist") [52] on the ranked comparison of the transcriptomes of CHIR-Mon
677 vs DMSO-Mon. NES and FDRq value is indicated. **C**. Summary of GSEA of the gene sets that
678 characterize the macrophage subsets identified in severe COVID-19 [23] [25] [24] on the ranked
679 comparison of the transcriptomes of CHIR-Mon vs. DMSO-Mon. FDRq values are indicated only if
680 FDRq>0.0; empty dots, Not Significant. **D**. Overlap between the genes upregulated (|log2FC|>1;
681 adjp<0.05) in CHIR-Mon (relative to M-CSF-Mon) and M-MØ-specific marker genes (left panel) and

682 genes downregulated (|log2FC|>1; adjp<0.05) in CHIR-Mon (relative to M-CSF-Mon) and GM-MØ-
683 specific marker genes (right panel), with indication of some shared genes. **E.** Overlap between the
684 genes upregulated or downregulated in CHIR-AMØ (|log2FC|>1 and adjp<0.05) and the
685 CD163+/LGMN+ pro-fibrotic macrophage cluster defined in EGAS00001005634 [23] (left panel), or the
686 gene sets of MAFB-dependent (middle panel) and MAFB-inhibited (right panel) genes defined in
687 GSE155719 [52]. **F**. Overlap between the genes upregulated or downregulated in CHIR-AMØ
688 (|log2FC|>1 and adjp<0.05, or just adjp<0.05) and the Alveolar Macrophage signature as defined in
689 EGAS00001005634 (AMØ1 and AMØ2 clusters) [23] (left panel), GSE155249 (TRAM1 and TRAM2
690 clusters) [25] (middle panel) or in [54] (right panel). **G.** Summary of GSEA of the indicated gene sets (from
691 GSE68061 and GSE188278) on the ranked comparison of the DMSO-AMØ and CHIR-AMØ
692 transcriptomes. FDRq values are indicated only if FDRq>0.0.
693
694 **Figure S3**. **A**. UMAP (Uniform Manifold Approximation and Projection) embedding of 21310 single-
695 cell transcriptomes from human lungs as reported in GSE128033 [47]. **B**. UMAP embedding of the
696 single-cell transcriptomes of computationally identified macrophages reported in GSE128033 [47]. **C**.
697 Color-coded expression of the indicated genes after projection onto the UMAP embedding shown
698 in **B**.
699
700 **SUPPLEMENTARY TABLES**
701 **Table S1**.- Transcriptional datasets used in the present study.
702

703 **REFERENCES**

704 1. Dick, S. A. *et al.* Three tissue resident macrophage subsets coexist across organs with
705 conserved origins and life cycles. *Sci. Immunol.* **7**, (2022).
706 2. Mulder, K. *et al.* Cross-tissue single-cell landscape of human monocytes and
707 macrophages in health and disease. *Immunity* **54**, 1883-1900.e5 (2021).
708 3. Hoeffel, G. & Ginhoux, F. Fetal monocytes and the origins of tissue-resident
709 macrophages. *Cell. Immunol.* **330**, 5–15 (2018).
710 4. Ruffell, B. & Coussens, L. M. Macrophages and therapeutic resistance in cancer.
711 *Cancer Cell* **27**, 462–472 (2015).
712 5. Lavin, Y., Mortha, A., Rahman, A. & Merad, M. Regulation of macrophage
713 development and function in peripheral tissues. *Nat Rev Immunol* **15**, 731–744 (2015).
714 6. Caescu, C. I. *et al.* Colony stimulating factor-1 receptor signaling networks inhibit
715 mouse macrophage inflammatory responses by induction of microRNA-21. *Blood* **125**,
716 e1–e13 (2015).
717 7. Van Overmeire, E. *et al.* M-CSF and GM-CSF Receptor Signaling Differentially Regulate
718 Monocyte Maturation and Macrophage Polarization in the Tumor Microenvironment.
719 *Cancer Res* **76**, 35–42 (2016).
720 8. Fleetwood, A. J., Lawrence, T., Hamilton, J. A. & Cook, A. D. Granulocyte-Macrophage
721 Colony-Stimulating Factor (CSF) and Macrophage CSF-Dependent Macrophage
722 Phenotypes Display Differences in Cytokine Profiles and Transcription Factor
723 Activities: Implications for CSF Blockade in Inflammation. *J. Immunol.* **178**, 5245–5252
724 (2007).
725 9. Lacey, D. C. *et al.* Defining GM-CSF- and Macrophage-CSF-Dependent Macrophage
726 Responses by In Vitro Models. *J Immunol* **188**, 5752–5765 (2012).
727 10. Gonzalez-Dominguez, E. *et al.* Atypical Activin A and IL-10 Production Impairs Human
728 CD16+ Monocyte Differentiation into Anti-Inflammatory Macrophages. *J Immunol*
729 **196**, 1327–1337 (2016).
730 11. Fleetwood, A. J., Dinh, H., Cook, A. D., Hertzog, P. J. & Hamilton, J. A. GM-CSF- and M-
731 CSF-dependent macrophage phenotypes display differential dependence on Type I
732 interferon signaling. *J. Leukoc. Biol.* **86**, 411–421 (2009).
733 12. Sierra-Filardi, E. *et al.* Activin A skews macrophage polarization by promoting a

734 proinflammatory phenotype and inhibiting the acquisition of anti-inflammatory
735 macrophage markers. *Blood* **117**, 5092–5101 (2011).
736 13. Gonzalez-Dominguez, E. *et al.* CD163L1 and CLEC5A discriminate subsets of human
737 resident and inflammatory macrophages in vivo. *J. Leukoc. Biol.* **98**, 453–466 (2015).
738 14. Palacios, B. S. *et al.* Macrophages from the synovium of active rheumatoid arthritis
739 exhibit an activin a-dependent pro-inflammatory profile. *J. Pathol.* **235**, 515–526
740 (2015).
741 15. de las Casas-Engel, M. *et al.* Serotonin Skews Human Macrophage Polarization
742 through HTR 2B and HTR 7 . *J. Immunol.* **190**, 2301–2310 (2013).
743 16. Nieto, C. *et al.* The activin A-peroxisome proliferator-activated receptor gamma axis
744 contributes to the transcriptome of GM-CSF-conditioned human macrophages. *Front.*
745 *Immunol.* **9**, (2018).
746 17. Guilliams, M. *et al.* Alveolar macrophages develop from fetal monocytes that
747 differentiate into long-lived cells in the first week of life via GM-CSF. *J Exp Med* **210**,
748 1977–1992 (2013).
749 18. Trapnell, B. C., Carey, B. C., Uchida, K. & Suzuki, T. Pulmonary alveolar proteinosis, a
750 primary immunodeficiency of impaired GM-CSF stimulation of macrophages. *Curr*
751 *Opin Immunol* **21**, 514–521 (2009).
752 19. Huang, X., Cao, M. & Xiao, Y. Alveolar macrophages in pulmonary alveolar proteinosis:
753 origin, function, and therapeutic strategies. *Front. Immunol.* **14**, (2023).
754 20. Donadon, M. *et al.* Macrophage morphology correlates with single-cell diversity and
755 prognosis in colorectal liver metastasis. *J. Exp. Med.* **217**, (2020).
756 21. Joshi, N. *et al.* A spatially restricted fibrotic niche in pulmonary fibrosis is sustained by
757 M-CSF/M-CSFR signalling in monocyte-derived alveolar macrophages. *Eur. Respir. J.*
758 **55**, 1–16 (2020).
759 22. Vega, M. A. *et al.* MAFB and MAF Transcription Factors as Macrophage Checkpoints
760 for COVID-19 Severity. *Front. Immunol.* **11**, (2020).
761 23. Wendisch, D. *et al.* SARS-CoV-2 infection triggers profibrotic macrophage responses
762 and lung fibrosis. *Cell* **184**, 6243-6261.e27 (2021).
763 24. Liao, M. *et al.* Single-cell landscape of bronchoalveolar immune cells in patients with
764 COVID-19. *Nat. Med.* **26**, 842–844 (2020).

765 25. Grant, R. A. *et al.* Circuits between infected macrophages and T cells in SARS-CoV-2
766 pneumonia. *Nature* **590**, 635–641 (2021).
767 26. Schultze, J. L. Reprogramming of macrophages - New opportunities for therapeutic
768 targeting. *Curr. Opin. Pharmacol.* **26**, 10–15 (2016).
769 27. Cuevas, V. D. *et al.* MAFB Determines Human Macrophage Anti-Inflammatory
770 Polarization: Relevance for the Pathogenic Mechanisms Operating in Multicentric
771 Carpotarsal Osteolysis. *J. Immunol.* **198**, 2070–2081 (2017).
772 28. Kim, H. The transcription factor MafB promotes anti-inflammatory M2 polarization
773 and cholesterol efflux in macrophages. *Sci. Rep.* **7**, (2017).
774 29. Kang, K. *et al.* Interferon-γ Represses M2 Gene Expression in Human Macrophages by
775 Disassembling Enhancers Bound by the Transcription Factor MAF. *Immunity* **47**, 235-
776 250.e4 (2017).
777 30. Eychène, A., Rocques, N. & Pouponnot, C. A new MAFia in cancer. *Nature Reviews*
778 *Cancer* vol. 8 683–693 (2008).
779 31. Lavin, Y. *et al.* Tissue-resident macrophage enhancer landscapes are shaped by the
780 local microenvironment. *Cell* **159**, 1312–1326 (2014).
781 32. Kelly, L. M., Englmeier, U., Lafon, I., Sieweke, M. H. & Graf, T. MafB is an inducer of
782 monocytic differentiation. *EMBO J.* **19**, 1987–1997 (2000).
783 33. Aziz, A., Soucie, E., Sarrazin, S. & Sieweke, M. H. MafB/c-Maf deficiency enables self-
784 renewal of differentiated functional macrophages. *Science (80-.).* **326**, 867–871
785 (2009).
786 34. Soucie, E. L. *et al.* Lineage-specific enhancers activate self-renewal genes in
787 macrophages and embryonic stem cells. *Science (80-.).* **351**, aad5510 (2016).
788 35. Sarrazin, S. *et al.* MafB restricts M-CSF-dependent myeloid commitment divisions of
789 hematopoietic stem cells. *Cell* **138**, 300–313 (2009).
790 36. Cuevas, V. D. *et al.* The gene signature of activated M-CSF-Primed human monocyte-
791 derived macrophages is IL-10-dependent. *J. Innate Immun.* (2021)
792 doi:10.1159/000519305.
793 37. Ríos, I. *et al.* GSK3β Inhibition Prevents Macrophage Reprogramming by High-Dose
794 Methotrexate. *J. Innate Immun.* 283–296 (2022) doi:10.1159/000526622.
795 38. de la Aleja, A. G. *et al.* Inhibition of LXR controls the polarization of human

796 inflammatory macrophages through upregulation of MAFB. *Cell. Mol. Life Sci.* **80**,
797 (2023).
798 39. Nagayoshi, R. *et al.* Effectiveness of anti-folate receptor β antibody conjugated with
799 truncated Pseudomonas exotoxin in the targeting of rheumatoid arthritis synovial
800 macrophages. *Arthritis Rheum.* **52**, 2666–2675 (2005).
801 40. Kim, D., Paggi, J. M., Park, C., Bennett, C. & Salzberg, S. L. Graph-based genome
802 alignment and genotyping with HISAT2 and HISAT-genotype. *Nat. Biotechnol.* **37**, 907–
803 915 (2019).
804 41. Langmead, B. & Salzberg, S. L. Fast gapped-read alignment with Bowtie 2. *Nat.*
805 *Methods* **9**, 357–359 (2012).
806 42. Anders, S., Pyl, P. T. & Huber, W. HTSeq-A Python framework to work with high-
807 throughput sequencing data. *Bioinformatics* **31**, 166–169 (2015).
808 43. Li, B. & Dewey, C. N. RSEM: Accurate transcript quantification from RNA-Seq data with
809 or without a reference genome. *BMC Bioinformatics* **12**, (2011).
810 44. Chen, E. Y. *et al.* Enrichr: Interactive and collaborative HTML5 gene list enrichment
811 analysis tool. *BMC Bioinformatics* **14**, 128 (2013).
812 45. Kuleshov, M. V *et al.* Enrichr: a comprehensive gene set enrichment analysis web
813 server 2016 update. *Nucleic Acids Res* **44**, W90–W97 (2016).
814 46. Subramanian, A. *et al.* Gene set enrichment analysis: a knowledge-based approach for
815 interpreting genome-wide expression profiles. *Proc Natl Acad Sci U S A* **102**, 15545–
816 15550 (2005).
817 47. Morse, C. *et al.* Proliferating SPP1/MERTK-expressing macrophages in idiopathic
818 pulmonary fibrosis. *Eur. Respir. J.* **54**, (2019).
819 48. Brand, M. D. & Nicholls, D. G. Assessing mitochondrial dysfunction in cells. *Biochem. J.*
820 **435**, 297–312 (2011).
821 49. Rueden, C. T. *et al.* ImageJ2: ImageJ for the next generation of scientific image data.
822 *BMC Bioinformatics* **18**, (2017).
823 50. Gutiérrez-Seijo, A. *et al.* Activin A Sustains the Metastatic Phenotype of Tumor-
824 Associated Macrophages and Is a Prognostic Marker in Human Cutaneous Melanoma.
825 *J. Invest. Dermatol.* **142**, 653-661.e2 (2022).
826 51. Garcia-Alonso, L., Holland, C. H., Ibrahim, M. M., Turei, D. & Saez-Rodriguez, J.

827 Benchmark and integration of resources for the estimation of human transcription
828 factor activities. *Genome Res.* **29**, 1363–1375 (2019).
829 52. Simón-Fuentes, M. *et al.* MAFB shapes human monocyte–derived macrophage
830 response to SARS-CoV-2 and controls severe COVID-19 biomarker expression. *JCI*
831 *Insight* **8**, (2023).
832 53. Wculek, S. K., Dunphy, G., Heras-Murillo, I., Mastrangelo, A. & Sancho, D. Metabolism
833 of tissue macrophages in homeostasis and pathology. *Cellular and Molecular*
834 *Immunology* vol. 19 384–408 (2022).
835 54. Melms, J. C. *et al.* A molecular single-cell lung atlas of lethal COVID-19. *Nature* **595**,
836 (2021).
837 55. Li, X. *et al.* ScRNA-seq expression of IFI27 and APOC2 identifies four alveolar
838 macrophage superclusters in healthy BALF. *Life Sci. Alliance* **5**, (2022).
839 56. González de la Aleja, A. *et al.* Activation of LXR Nuclear Receptors Impairs the Anti-
840 Inflammatory Gene and Functional Profile of M-CSF-Dependent Human Monocyte-
841 Derived Macrophages. *Front. Immunol.* **13**, (2022).
842 57. Domínguez-Soto, Á. *et al.* IVIg Promote Cross-Tolerance against Inflammatory Stimuli
843 In Vitro and In Vivo. *J. Immunol.* **201**, 41–52 (2018).
844 58. Molgora, M. & Colonna, M. Turning enemies into allies—reprogramming tumor-
845 associated macrophages for cancer therapy. *Med* vol. 2 666–681 (2021).
846 59. Zheng, W. & Pollard, J. W. Inhibiting macrophage PI3K? To enhance immunotherapy.
847 *Cell Res.* **26**, 1267–1268 (2016).
848 60. Kaneda, M. M. *et al.* PI3Kγ 3 is a molecular switch that controls immune suppression.
849 *Nature* **539**, 437–442 (2016).
850 61. Byles, V. *et al.* The TSC-mTOR pathway regulates macrophage polarization. *Nat.*
851 *Commun.* **4**, (2013).
852 62. Do, M. H. *et al.* Reprogramming tumor-associated macrophages to outcompete
853 endovascular endothelial progenitor cells and suppress tumor neoangiogenesis.
854 *Immunity* **56**, 2555-2569.e5 (2023).
855 63. Zhang, X. *et al.* Reprogramming tumour-associated macrophages to outcompete
856 cancer cells. *Nature* **619**, 616–623 (2023).
857 64. Evangelisti, C., Chiarini, F., Paganelli, F., Marmiroli, S. & Martelli, A. M. Crosstalks of

858 GSK3 signaling with the mTOR network and effects on targeted therapy of cancer.
859 *Biochimica et Biophysica Acta - Molecular Cell Research* vol. 1867 (2020).
860 65. Rodionova, E. *et al.* GSK-3 mediates differentiation and activation of proinflammatory
861 dendritic cells. *Blood* **109**, 1584–1592 (2007).
862 66. Bakri, Y. *et al.* Balance of MafB and PU.1 specifies alternative macrophage or dendritic
863 cell fate. *Blood* **105**, 2707–2716 (2005).
864 67. Delorey, T. M. *et al.* COVID-19 tissue atlases reveal SARS-CoV-2 pathology and cellular
865 targets. *Nature* **595**, 107–113 (2021).
866 68. Koshida, R., Oishi, H., Hamada, M. & Takahashi, S. MafB antagonizes phenotypic
867 alteration induced by GM-CSF in microglia. *Biochem Biophys Res Commun* **463**, 109–
868 115 (2015).
869 69. Lang, F. M., Lee, K. M. C., Teijaro, J. R., Becher, B. & Hamilton, J. A. GM-CSF-based
870 treatments in COVID-19: reconciling opposing therapeutic approaches. *Nat. Rev.*
871 *Immunol.* (2020) doi:10.1038/s41577-020-0357-7.
872 70. Bosteels, C. *et al.* Loss of GM-CSF-dependent instruction of alveolar macrophages in
873 COVID-19 provides a rationale for inhaled GM-CSF treatment. *Cell Reports Med.* **3**,
874 (2022).
875

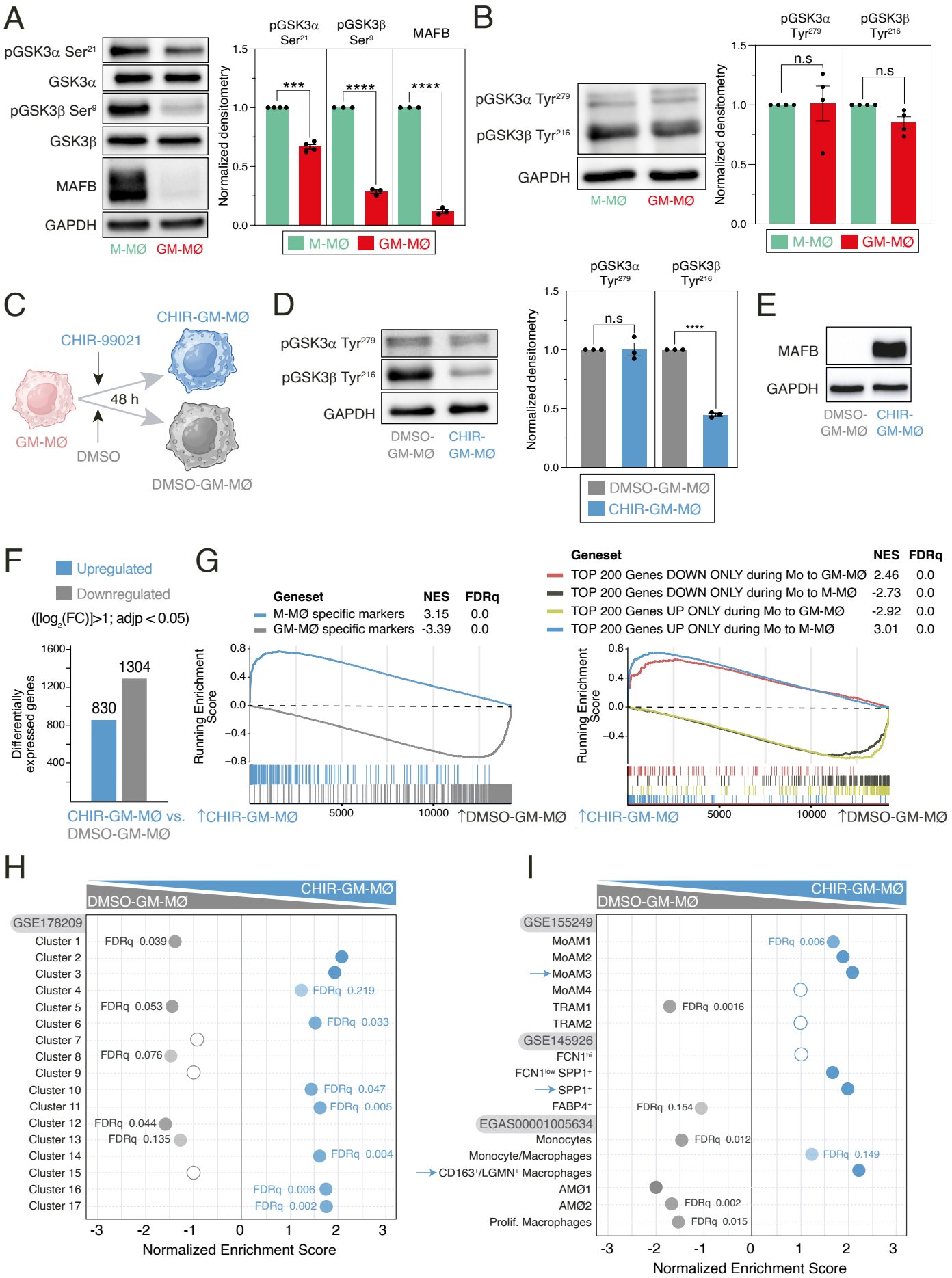
A
pGSK3α Ser21
GSK3α
pGSK3β Ser9
GSK3β
MAFB
GAPDH
M-MØ GM-MØ
pGSK3α Ser21
pGSK3β Ser9
MAFB
Normalized densitometry
***
****
****
M-MØ GM-MØ
B
pGSK3α Tyr279
pGSK3β Tyr216
GAPDH
M-MØ GM-MØ
pGSK3α Tyr279
pGSK3β Tyr216
n.s
n.s
Normalized densitometry
M-MØ GM-MØ
C
CHIR-GM-MØ
CHIR-99021
48 h
GM-MØ
DMSO
DMSO-GM-MØ
D
pGSK3α Tyr279
pGSK3β Tyr216
GAPDH
DMSO-GM-MØ
CHIR-GM-MØ
pGSK3α Tyr279
pGSK3β Tyr216
n.s
****
Normalized densitometry
DMSO-GM-MØ
CHIR-GM-MØ
E
MAFB
GAPDH
DMSO-GM-MØ
CHIR-GM-MØ
F
Upregulated
Downregulated
([log2(FC)]>1; adjp < 0.05)
Differentially expressed genes
830
1304
CHIR-GM-MØ vs. DMSO-GM-MØ
G
Geneset NES FDRq
M-MØ specific markers 3.15 0.0
GM-MØ specific markers -3.39 0.0
Running Enrichment Score
↑CHIR-GM-MØ
↑DMSO-GM-MØ
Geneset NES FDRq
TOP 200 Genes DOWN ONLY during Mo to GM-MØ 2.46 0.0
TOP 200 Genes DOWN ONLY during Mo to M-MØ -2.73 0.0
TOP 200 Genes UP ONLY during Mo to GM-MØ -2.92 0.0
TOP 200 Genes UP ONLY during Mo to M-MØ 3.01 0.0
Running Enrichment Score
↑CHIR-GM-MØ
↑DMSO-GM-MØ
H
CHIR-GM-MØ
DMSO-GM-MØ
GSE178209
Cluster 1 FDRq 0.039
Cluster 2
Cluster 3
Cluster 4 FDRq 0.219
Cluster 5 FDRq 0.053
Cluster 6 FDRq 0.033
Cluster 7
Cluster 8 FDRq 0.076
Cluster 9
Cluster 10 FDRq 0.047
Cluster 11 FDRq 0.005
Cluster 12 FDRq 0.044
Cluster 13 FDRq 0.135
Cluster 14 FDRq 0.004
Cluster 15
Cluster 16 FDRq 0.006
Cluster 17 FDRq 0.002
Normalized Enrichment Score
I
CHIR-GM-MØ
DMSO-GM-MØ
GSE155249
MoAM1 FDRq 0.006
MoAM2
MoAM3
MoAM4
TRAM1 FDRq 0.0016
TRAM2
GSE145926
FCN1hi
FCN1low SPP1+
SPP1+
FABP4+ FDRq 0.154
EGAS00001005634
Monocytes FDRq 0.012
Monocyte/Macrophages FDRq 0.149
CD163+/LGMN+ Macrophages
AMØ1
AMØ2 FDRq 0.002
Prolif. Macrophages FDRq 0.015
Normalized Enrichment Score

Figure 1

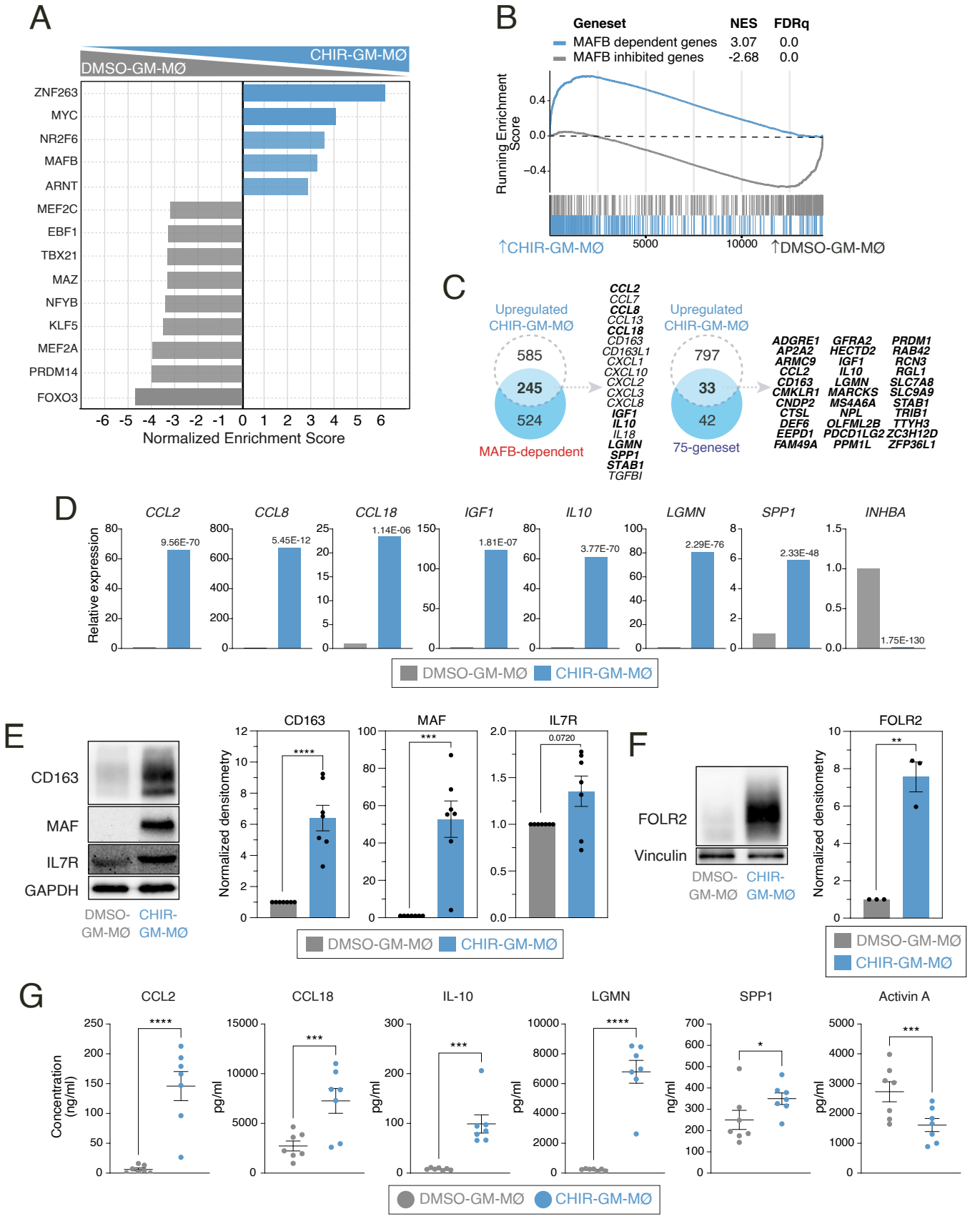
A
CHIR-GM-MØ
DMSO-GM-MØ
ZNF263
MYC
NR2F6
MAFB
ARNT
MEF2C
EBF1
TBX21
MAZ
NFYB
KLF5
MEF2A
PRDM14
FOXO3
-6 -5 -4 -3 -2 -1 0 1 2 3 4 5 6
Normalized Enrichment Score
B
Geneset NES FDRq
MAFB dependent genes 3.07 0.0
MAFB inhibited genes -2.68 0.0
Running Enrichment Score
0.4
0.0
−0.4
↑CHIR-GM-MØ
5000
10000
↑DMSO-GM-MØ
C
Upregulated CHIR-GM-MØ
585
245
524
MAFB-dependent
CCL2 CCL7 CCL8 CCL13 CCL18 CD163 CD163L1 CXCL1 CXCL10 CXCL2 CXCL3 CXCL8 IGF1 IL10 IL18 LGMN SPP1 STAB1 TGFBI
Upregulated CHIR-GM-MØ
797
33
42
75-geneset
ADGRE1 AP2A2 ARMC9 CCL2 CD163 CMKLR1 CNDP2 CTSL DEF6 EEPD1 FAM49A
GFRA2 HECTD2 IGF1 IL10 LGMN MARCKS MS4A6A NPL OLFML2B PDCD1LG2 PPM1L
PRDM1 RAB42 RCN3 RGL1 SLC7A8 SLC9A9 STAB1 TRIB1 TTYH3 ZC3H12D ZFP36L1
D
CCL2 CCL8 CCL18 IGF1 IL10 LGMN SPP1 INHBA
Relative expression
9.56E-70
5.45E-12
1.14E-06
1.81E-07
3.77E-70
2.29E-76
2.33E-48
1.75E-130
DMSO-GM-MØ CHIR-GM-MØ
E
CD163
MAF
IL7R
GAPDH
DMSO-GM-MØ CHIR-GM-MØ
CD163 MAF IL7R
Normalized densitometry
****
***
0.0720
DMSO-GM-MØ CHIR-GM-MØ
F
FOLR2
Vinculin
DMSO-GM-MØ CHIR-GM-MØ
FOLR2
Normalized densitometry
**
DMSO-GM-MØ
CHIR-GM-MØ
G
CCL2 CCL18 IL-10 LGMN SPP1 Activin A
Concentration (ng/ml)
pg/ml
ng/ml
****
***
*
DMSO-GM-MØ CHIR-GM-MØ

Figure 2

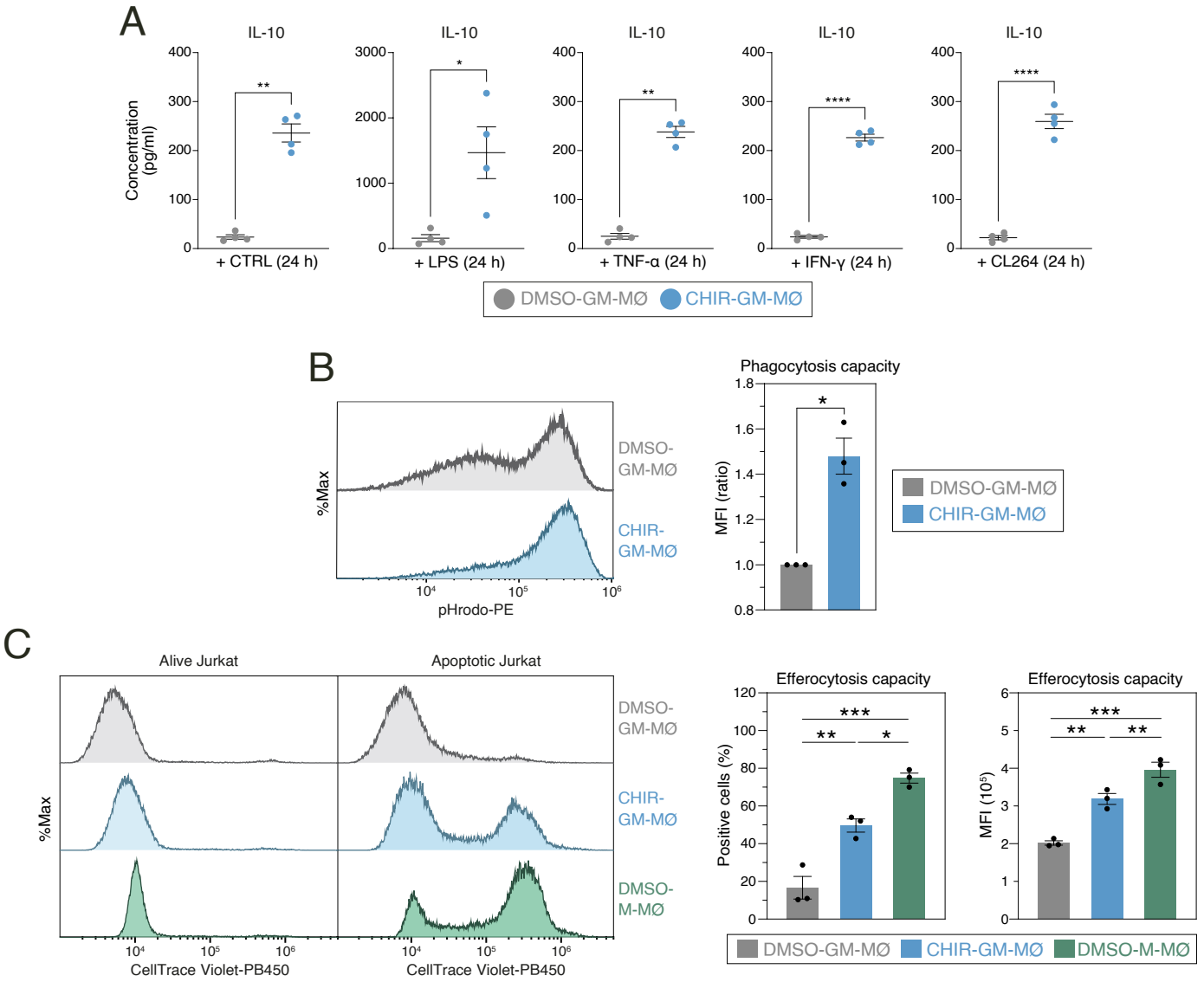
A
IL-10
Concentration (pg/ml)
+ CTRL (24 h)
+ LPS (24 h)
+ TNF-α (24 h)
+ IFN-γ (24 h)
+ CL264 (24 h)
DMSO-GM-MØ
CHIR-GM-MØ
B
%Max
pHrodo-PE
Phagocytosis capacity
MFI (ratio)
C
Alive Jurkat
Apoptotic Jurkat
CellTrace Violet-PB450
Efferocytosis capacity
Positive cells (%)
MFI (10⁵)
DMSO-M-MØ

Figure 3

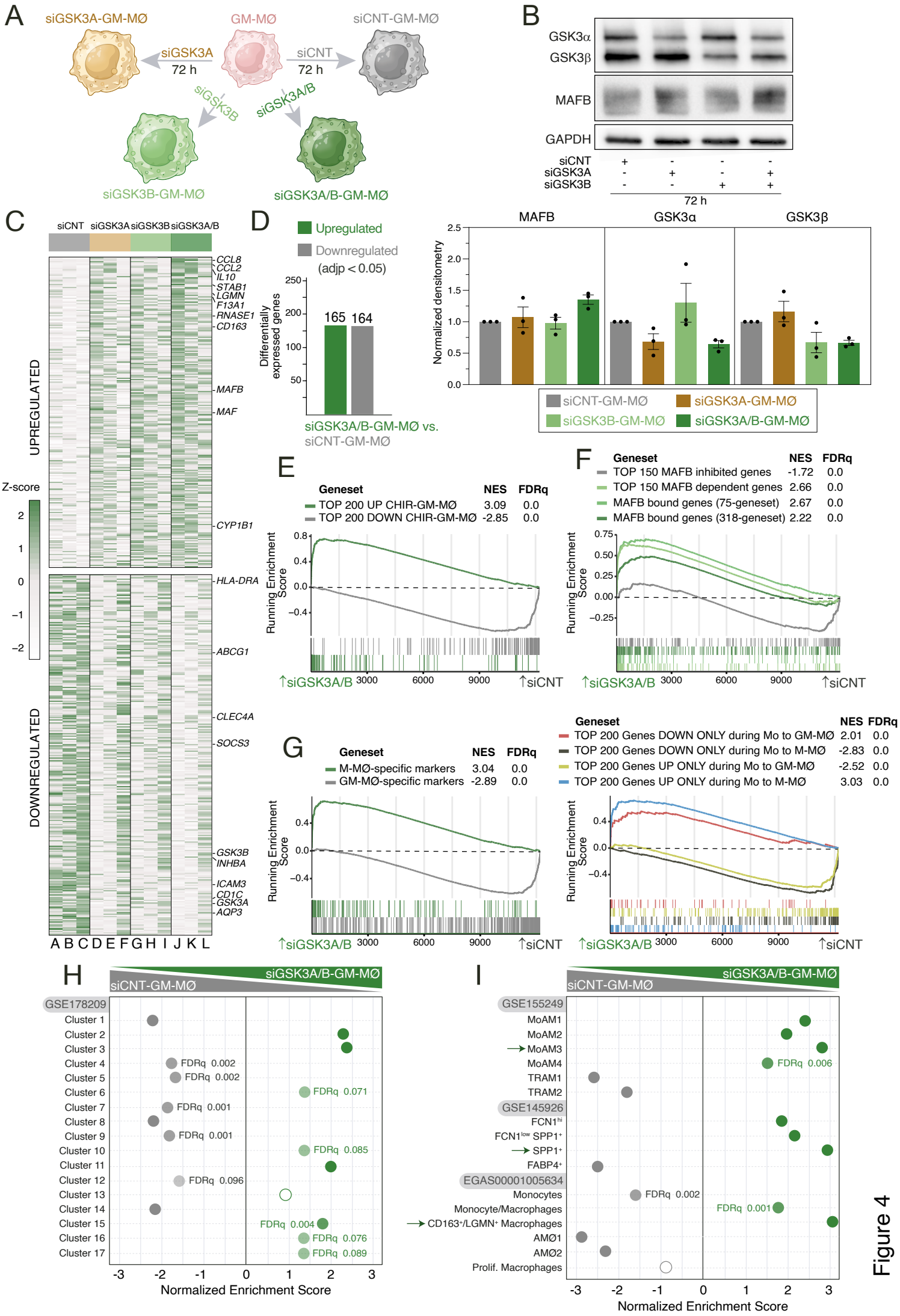
A
siGSK3A-GM-MØ
GM-MØ
siCNT-GM-MØ
siGSK3A
72 h
siCNT
72 h
siGSK3B
siGSK3A/B
siGSK3B-GM-MØ
siGSK3A/B-GM-MØ
B
GSK3α
GSK3β
MAFB
GAPDH
siCNT
siGSK3A
siGSK3B
72 h
C
siCNT siGSK3A siGSK3B siGSK3A/B
UPREGULATED
DOWNREGULATED
Z-score
CCL8
CCL2
IL10
STAB1
LGMN
F13A1
RNASE1
CD163
MAFB
MAF
CYP1B1
HLA-DRA
ABCG1
CLEC4A
SOCS3
GSK3B
INHBA
ICAM3
CD1C
GSK3A
AQP3
A B C D E F G H I J K L
D
Upregulated
Downregulated
(adjp < 0.05)
Differentially expressed genes
165 164
siGSK3A/B-GM-MØ vs. siCNT-GM-MØ
MAFB
GSK3α
GSK3β
Normalized densitometry
siCNT-GM-MØ
siGSK3A-GM-MØ
siGSK3B-GM-MØ
siGSK3A/B-GM-MØ
E
Geneset NES FDRq
TOP 200 UP CHIR-GM-MØ 3.09 0.0
TOP 200 DOWN CHIR-GM-MØ -2.85 0.0
Running Enrichment Score
↑siGSK3A/B
↑siCNT
F
Geneset NES FDRq
TOP 150 MAFB inhibited genes -1.72 0.0
TOP 150 MAFB dependent genes 2.66 0.0
MAFB bound genes (75-geneset) 2.67 0.0
MAFB bound genes (318-geneset) 2.22 0.0
Running Enrichment Score
↑siGSK3A/B
↑siCNT
G
Geneset NES FDRq
M-MØ-specific markers 3.04 0.0
GM-MØ-specific markers -2.89 0.0
Geneset NES FDRq
TOP 200 Genes DOWN ONLY during Mo to GM-MØ 2.01 0.0
TOP 200 Genes DOWN ONLY during Mo to M-MØ -2.83 0.0
TOP 200 Genes UP ONLY during Mo to GM-MØ -2.52 0.0
TOP 200 Genes UP ONLY during Mo to M-MØ 3.03 0.0
Running Enrichment Score
↑siGSK3A/B
↑siCNT
H
siCNT-GM-MØ
siGSK3A/B-GM-MØ
GSE178209
Cluster 1
Cluster 2
Cluster 3
Cluster 4 FDRq 0.002
Cluster 5 FDRq 0.002
Cluster 6 FDRq 0.071
Cluster 7 FDRq 0.001
Cluster 8
Cluster 9 FDRq 0.001
Cluster 10 FDRq 0.085
Cluster 11
Cluster 12 FDRq 0.096
Cluster 13
Cluster 14
Cluster 15 FDRq 0.004
Cluster 16 FDRq 0.076
Cluster 17 FDRq 0.089
Normalized Enrichment Score
I
siCNT-GM-MØ
siGSK3A/B-GM-MØ
GSE155249
MoAM1
MoAM2
MoAM3
MoAM4 FDRq 0.006
TRAM1
TRAM2
GSE145926
FCN1hi
FCN1low SPP1+
SPP1+
FABP4+
EGAS00001005634
Monocytes FDRq 0.002
Monocyte/Macrophages FDRq 0.001
CD163+/LGMN+ Macrophages
AMØ1
AMØ2
Prolif. Macrophages
Normalized Enrichment Score

Figure 4

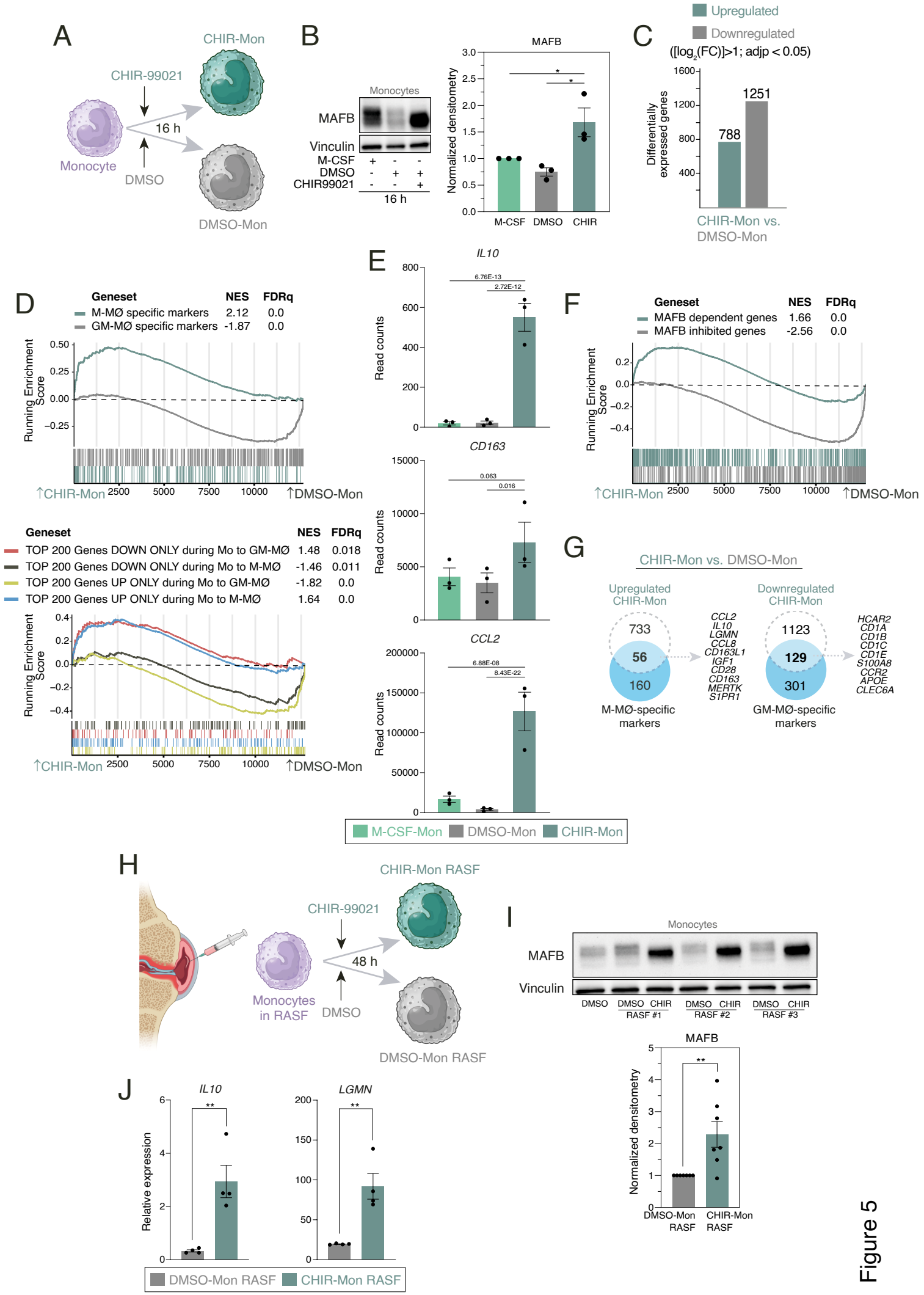
A
CHIR-Mon
CHIR-99021
16 h
Monocyte
DMSO
DMSO-Mon
B
Monocytes
MAFB
Vinculin
M-CSF + - -
DMSO - + +
CHIR99021 - - +
16 h
MAFB
Normalized densitometry
M-CSF DMSO CHIR
C
Upregulated
Downregulated
([log2(FC)]>1; adjp < 0.05)
Differentially expressed genes
788
1251
CHIR-Mon vs. DMSO-Mon
D
Geneset NES FDRq
M-MØ specific markers 2.12 0.0
GM-MØ specific markers -1.87 0.0
Running Enrichment Score
↑CHIR-Mon
↑DMSO-Mon
Geneset NES FDRq
TOP 200 Genes DOWN ONLY during Mo to GM-MØ 1.48 0.018
TOP 200 Genes DOWN ONLY during Mo to M-MØ -1.46 0.011
TOP 200 Genes UP ONLY during Mo to GM-MØ -1.82 0.0
TOP 200 Genes UP ONLY during Mo to M-MØ 1.64 0.0
E
IL10
CD163
CCL2
Read counts
6.76E-13
2.72E-12
0.063
0.016
6.88E-08
8.43E-22
M-CSF-Mon DMSO-Mon CHIR-Mon
F
Geneset NES FDRq
MAFB dependent genes 1.66 0.0
MAFB inhibited genes -2.56 0.0
G
CHIR-Mon vs. DMSO-Mon
Upregulated CHIR-Mon
733
56
160
M-MØ-specific markers
CCL2 IL10 LGMN CCL8 CD163L1 IGF1 CD28 CD163 MERTK S1PR1
Downregulated CHIR-Mon
1123
129
301
GM-MØ-specific markers
HCAR2 CD1A CD1B CD1C CD1E S100A8 CCR2 APOE CLEC6A
H
CHIR-Mon RASF
CHIR-99021
48 h
Monocytes in RASF
DMSO
DMSO-Mon RASF
I
Monocytes
MAFB
Vinculin
DMSO DMSO CHIR RASF #1 DMSO CHIR RASF #2 DMSO CHIR RASF #3
MAFB
Normalized densitometry
DMSO-Mon RASF CHIR-Mon RASF
J
IL10
LGMN
Relative expression
DMSO-Mon RASF CHIR-Mon RASF

Figure 5

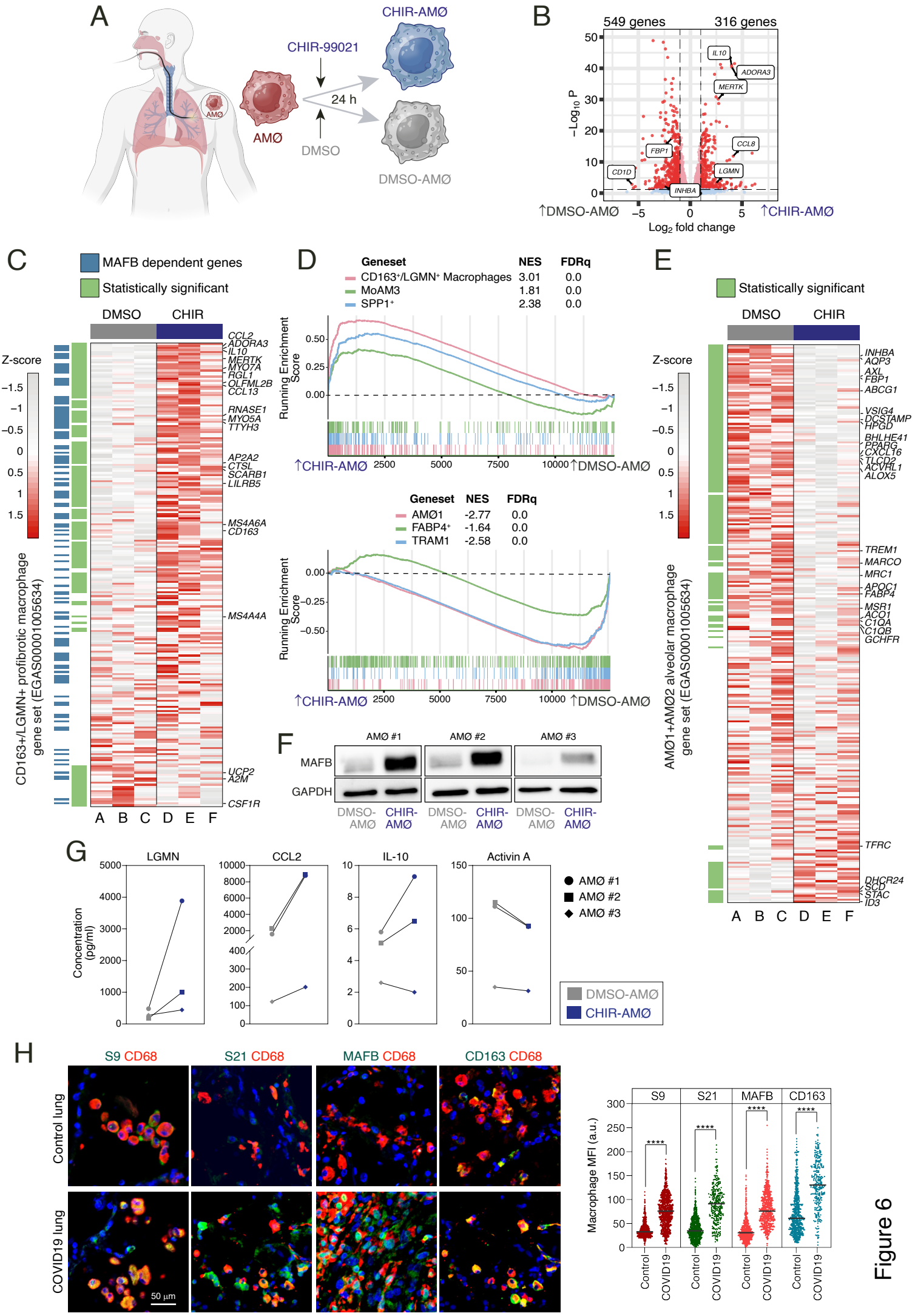
A
CHIR-AMØ
CHIR-99021
24 h
AMØ
DMSO
DMSO-AMØ
B
549 genes
316 genes
IL10
ADORA3
MERTK
CCL8
FBP1
CD1D
LGMN
INHBA
−Log10 P
↑DMSO-AMØ
↑CHIR-AMØ
Log2 fold change
C
MAFB dependent genes
Statistically significant
DMSO
CHIR
Z-score
CCL2
ADORA3
IL10
MERTK
MYO7A
RGL1
OLFML2B
CCL13
RNASE1
MYO5A
TTYH3
AP2A2
CTSL
SCARB1
LILRB5
MS4A6A
CD163
MS4A4A
UCP2
A2M
CSF1R
CD163+/LGMN+ profibrotic macrophage gene set (EGAS00001005634)
D
Geneset NES FDRq
CD163+/LGMN+ Macrophages 3.01 0.0
MoAM3 1.81 0.0
SPP1+ 2.38 0.0
Running Enrichment Score
Geneset NES FDRq
AMØ1 -2.77 0.0
FABP4+ -1.64 0.0
TRAM1 -2.58 0.0
E
Statistically significant
INHBA
AQP3
AXL
FBP1
ABCG1
VSIG4
DCSTAMP
HPGD
BHLHE41
PPARG
CXCL16
TLCD2
ACVRL1
ALOX5
TREM1
MARCO
MRC1
APOC1
FABP4
MSR1
ACO1
C1QA
C1QB
GCHFR
TFRC
DHCR24
SCD
STAC
ID3
AMØ1+AMØ2 alveolar macrophage gene set (EGAS00001005634)
F
AMØ #1
AMØ #2
AMØ #3
MAFB
GAPDH
DMSO-AMØ
CHIR-AMØ
G
LGMN
CCL2
IL-10
Activin A
Concentration (pg/ml)
AMØ #1
AMØ #2
AMØ #3
DMSO-AMØ
CHIR-AMØ
H
S9 CD68
S21 CD68
MAFB CD68
CD163 CD68
Control lung
COVID19 lung
50 µm
Macrophage MFI (a.u.)
S9
S21
MAFB
CD163
Control
COVID19

Figure 6

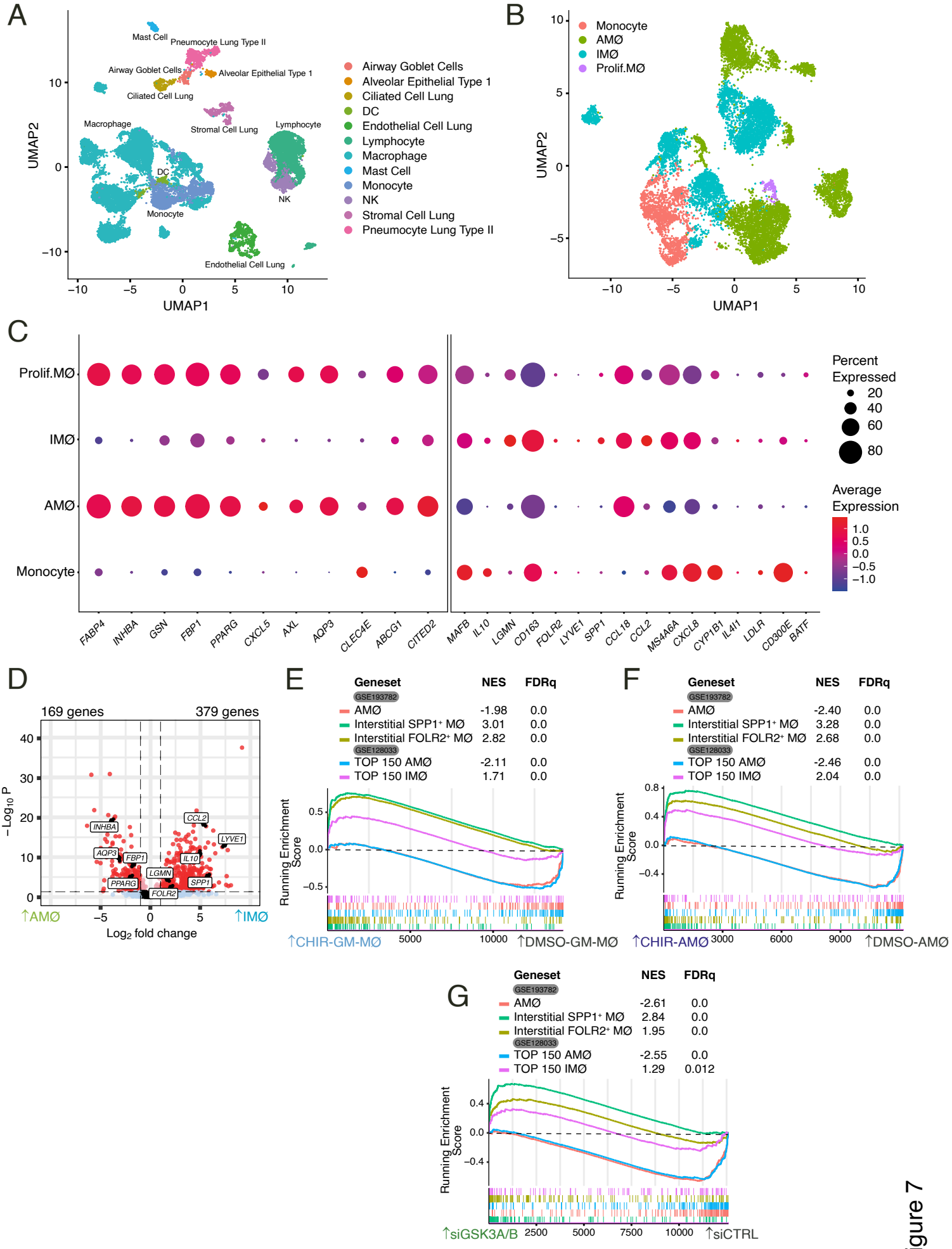
A
Mast Cell
Pneumocyte Lung Type II
Airway Goblet Cells
Alveolar Epithelial Type 1
Ciliated Cell Lung
Macrophage
Stromal Cell Lung
Lymphocyte
DC
NK
Monocyte
Endothelial Cell Lung
UMAP2
UMAP1
Airway Goblet Cells
Alveolar Epithelial Type 1
Ciliated Cell Lung
DC
Endothelial Cell Lung
Lymphocyte
Macrophage
Mast Cell
Monocyte
NK
Stromal Cell Lung
Pneumocyte Lung Type II
B
Monocyte
AMØ
IMØ
Prolif.MØ
UMAP2
UMAP1
C
Prolif.MØ
IMØ
AMØ
Monocyte
FABP4
INHBA
GSN
FBP1
PPARG
CXCL5
AXL
AQP3
CLEC4E
ABCG1
CITED2
MAFB
IL10
LGMN
CD163
FOLR2
LYVE1
SPP1
CCL18
CCL2
MS4A6A
CXCL8
CYP1B1
IL4I1
LDLR
CD300E
BATF
Percent Expressed
20
40
60
80
Average Expression
1.0
0.5
0.0
−0.5
−1.0
D
169 genes
379 genes
−Log10 P
INHBA
AQP3
FBP1
PPARG
LGMN
FOLR2
CCL2
IL10
SPP1
LYVE1
↑AMØ
↑IMØ
Log2 fold change
E
Geneset
NES
FDRq
GSE193782
AMØ -1.98 0.0
Interstitial SPP1+ MØ 3.01 0.0
Interstitial FOLR2+ MØ 2.82 0.0
GSE128033
TOP 150 AMØ -2.11 0.0
TOP 150 IMØ 1.71 0.0
Running Enrichment Score
↑CHIR-GM-MØ
↑DMSO-GM-MØ
F
Geneset
NES
FDRq
GSE193782
AMØ -2.40 0.0
Interstitial SPP1+ MØ 3.28 0.0
Interstitial FOLR2+ MØ 2.68 0.0
GSE128033
TOP 150 AMØ -2.46 0.0
TOP 150 IMØ 2.04 0.0
Running Enrichment Score
↑CHIR-AMØ
↑DMSO-AMØ
G
Geneset
NES
FDRq
GSE193782
AMØ -2.61 0.0
Interstitial SPP1+ MØ 2.84 0.0
Interstitial FOLR2+ MØ 1.95 0.0
GSE128033
TOP 150 AMØ -2.55 0.0
TOP 150 IMØ 1.29 0.012
Running Enrichment Score
↑siGSK3A/B
↑siCTRL

Figure 7